Enclosure 5

Report of an Independent Assessment of the Calculation of TSP Forces

Introduction

The investigation reported here was directed at answering the following two questions.

1. Can the forces on an orifice plate resulting from the transient, blowdown-type flow of a compressible fluid in a pipe be calculated from a form-loss?

2. Using a method other than finite differences, how can the pressures and velocities needed to determine such forces be calculated?

We have concluded that the answer to the first question is "yes". In what follows three independent analyses are presented in answer to the second question. However, before getting into these details the following more general comments should be made.

At the outset of the investigation a literature search was made to determine whether or not the characterization of an orifice be a form loss was appropriate under transient conditions. The consensus of several papers is that it is. Reference (1) is typical of these and includes experimental verification. A copy of this paper is included in this report. At the same time the appropriateness of using the same method of analysis in both compressible and incompressible flows was also considered. Reference (2) is submitted in support of the conclusion that it can.

The general characteristics of the three analyses of unsteady pipe flows should also be described. The first of these is by far the simplest, most direct and easiest to apply. It is, in fact, identical to the standard analysis of water hammer (see (1)) except that the sound speed and other physical properties of the fluid are those of a gas. It's drawback is that it is no doubt limited to some extent to weak waves in which the fluid can be considered quasi-incompressible.

The second analysis is the most general and also the most complex. In it the fluid is treated as completely compressible. This approach applies the theory of characteristics in the flow away from the orifice and the open end. These regions are then treated by assuming steady flow and applying the basic conservation laws. Treatment of the orifice in this manner does not require supplemental empirical information such as the orifice coefficient K. In fact K can be deduced from the results. This analysis is better suited to strong waves and also provides a check on the more direct approach. It is also better suited to a numerical calculation of the long-time conditions in the pipe.

The third analysis is a compromise between the other two. Compressibility is included but the orifice K-factor must be known.

All three of these analyses show that the pressure drop across the orifice is always given by an expression of the form

$$\Delta p = K \frac{\rho}{g} \frac{u^2}{2}$$

All three analyses agree with regard to the calculated values the fluid velocity and its pressure for the low Mach number case considered. The K-factor determined from the results of the second analysis verifies the value used in the other two.

It is recommended that caution be used in applying these findings to the results of finite difference calculations. The velocity through the orifice is critically dependent on the reflection and transmission of the wave at the orifice. In our experience finite difference calculations are not reliable in this respect. Thus we strongly recommend that you run our two test cases on your program and compare the results with those presented in Figure A7 of the text. The "reservoir" case can be

simulated by using an upstream pipe diameter equal to 100 times the downstream value.

A. Quasi-Incompressible Analysis

Density changes in forced gas flows in which the velocity does not exceed thirty percent of the local sound speed are not large (3). It is therefore expected that an analysis that treats the gas as incompressible, but with a finite sound speed will be valid over a significant range. The following analysis assumes these conditions. Two different cases are considered. In the first the orifice is assumed to be located somewhere in the middle of a long pipe. Thus flow on both sides is unsteady. In the second case the orifice is considered to be located at the entrance to the pipe from a reservoir sufficiently large so that the upstream conditions remain constant.

Pipe Problem

Consider a wave travelling to the right as shown below:

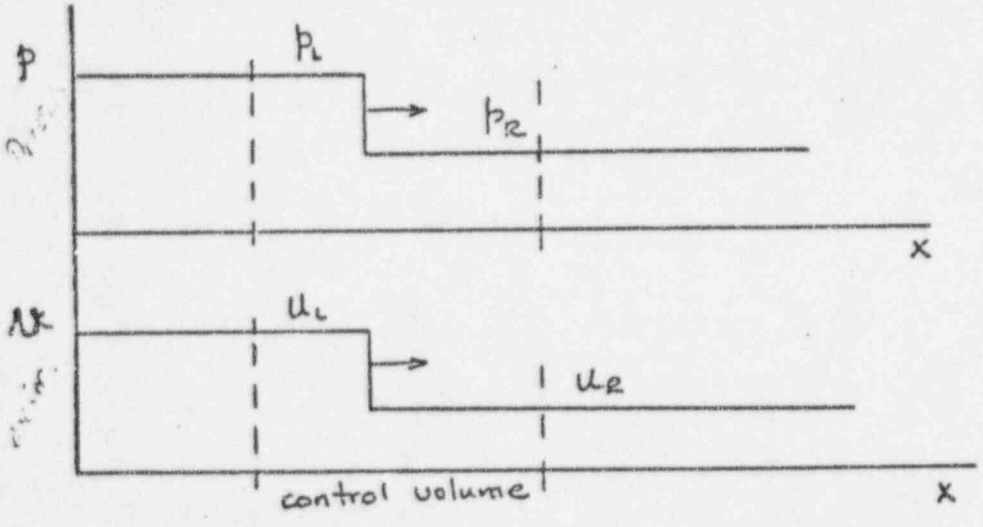

Figure A1

Applying a momentum balance to the control volume indicated:

$$\left(p_L + \frac{\rho}{g} u_L^2\right) - \left(p_R + \frac{\rho}{g} u_R^2\right) = \{\text{rate of change of momentum}\}.$$

But because the wave is moving to the right with wave-velocity a, $\frac{\rho}{g} a \delta t$ mass of fluid is accelerated from u_R to u_L in time dt. Thus,

$$\left\{\text{rate of change of momentum}\right\} = \frac{\rho}{g} \frac{a \delta t (u_L - u_R)}{\delta t}$$

Therefore $$\left(p_L + \frac{\rho}{g} u_L^2\right) - \left(p_R + \frac{\rho}{g} u_R^2\right) = \frac{\rho}{g} a (u_L - u_R)$$

$$p_L - p_R = \frac{\rho}{g} a \left(u_L - u_R + \frac{u_R^2 - u_L^2}{a}\right)$$

$$p_L - p_R = \frac{\rho}{g} a (u_L - u_R)\left(1 - \frac{u_R + u_L}{a}\right) \quad \text{(A1)}$$

Now if the wave is moving to the left, a mass of fluid goes from u_R to u_L. The only effect is to reverse the sign of the rate of change of momentum term:

$$p_L - p_R = \frac{\rho}{g} a (u_L - u_R)\left(-1 + \frac{u_R + u_L}{a}\right) \quad \text{(A2)}$$

Now consider an initially uniform and stationary fluid.

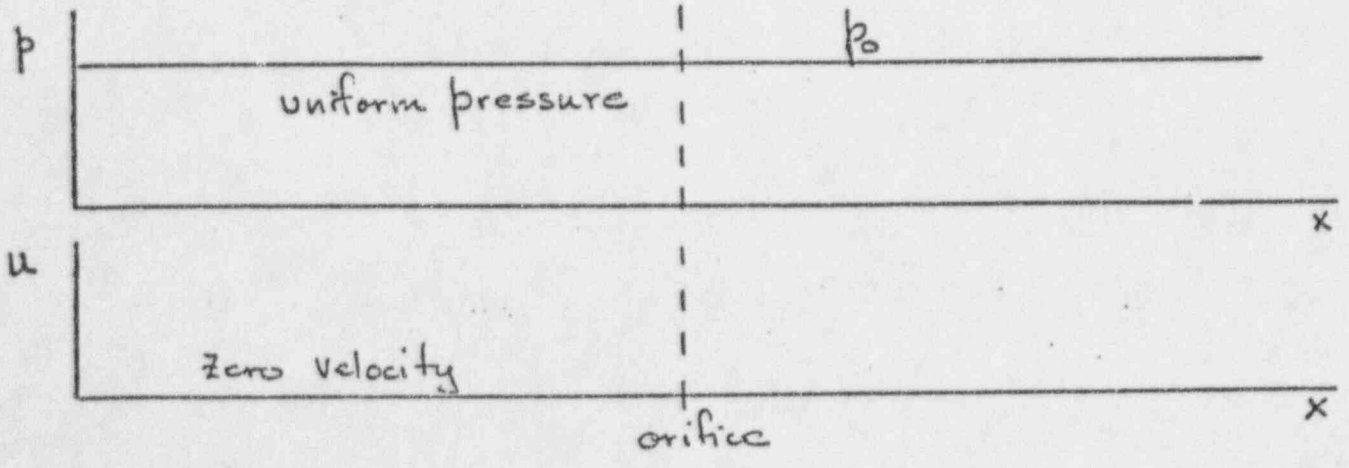

Figure A2

At some time the fluid at the right is accelerated to u_1 and a decompression wave starts down the tube:

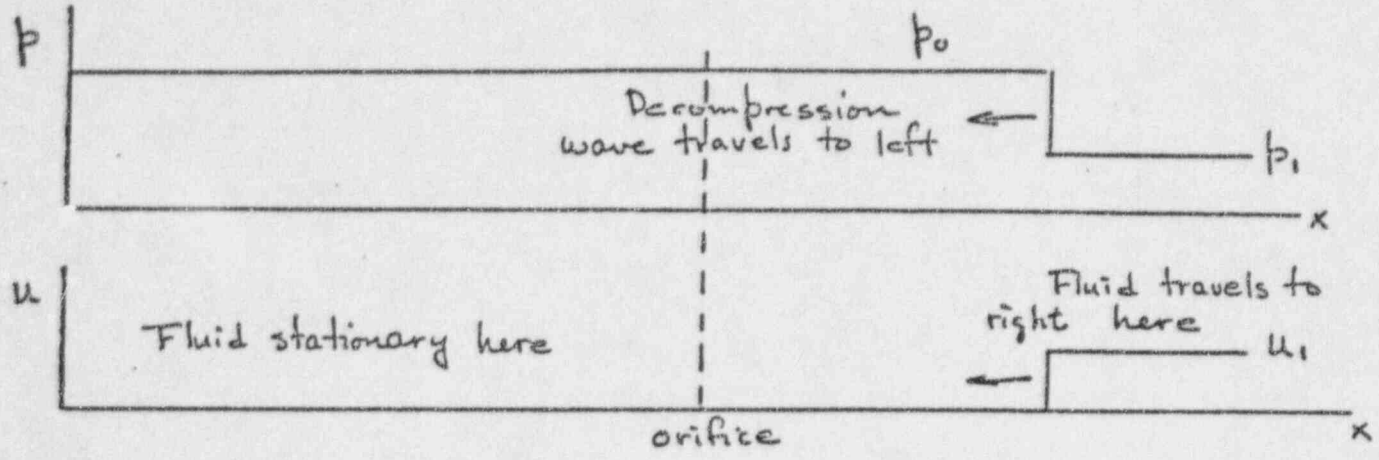

Figure A3

Using equation (A2), with $p_L = p_0$, $p_R = p_1$, $u_R = u_1$ and $u_L = u_0 = 0$

$$p_0 - p_1 = \frac{\rho}{g} a (-u_1) \left[\frac{u_0}{a} - 1 \right] \qquad \text{(A3)}$$

If $u_0 << a$, the u_0/a term in the brackets is negligible and we drop it in what follows. So

$$p_0 - p_1 \approx \frac{\rho}{g} a u_1 \qquad \text{(A4)}$$

FigureA3 applies until the left-travelling wave hits the orifice; we have:

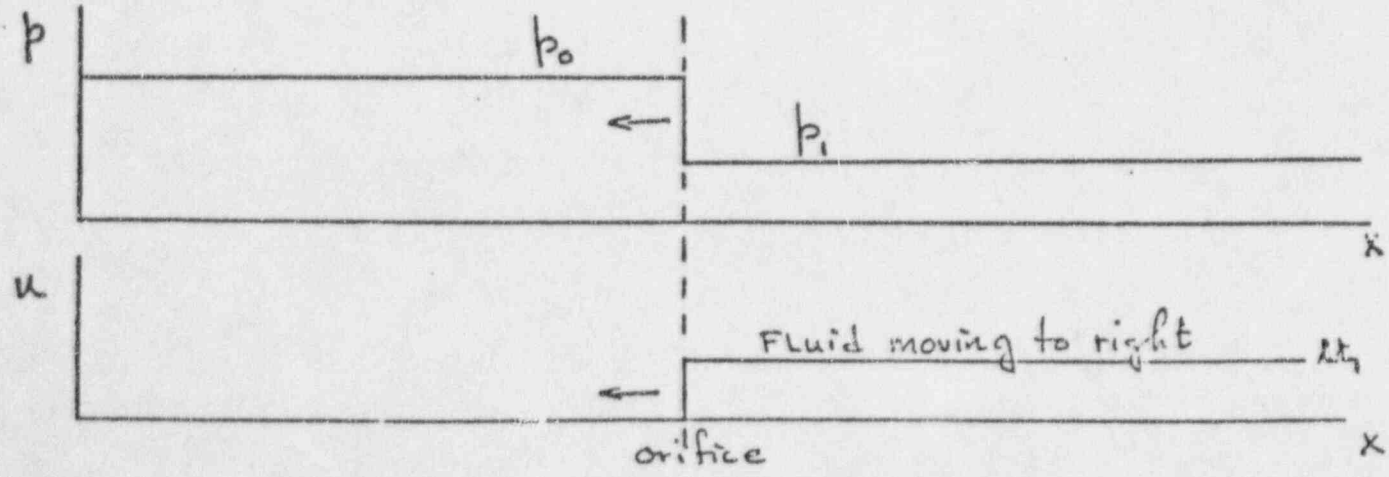

Figure A4

and just after, we have

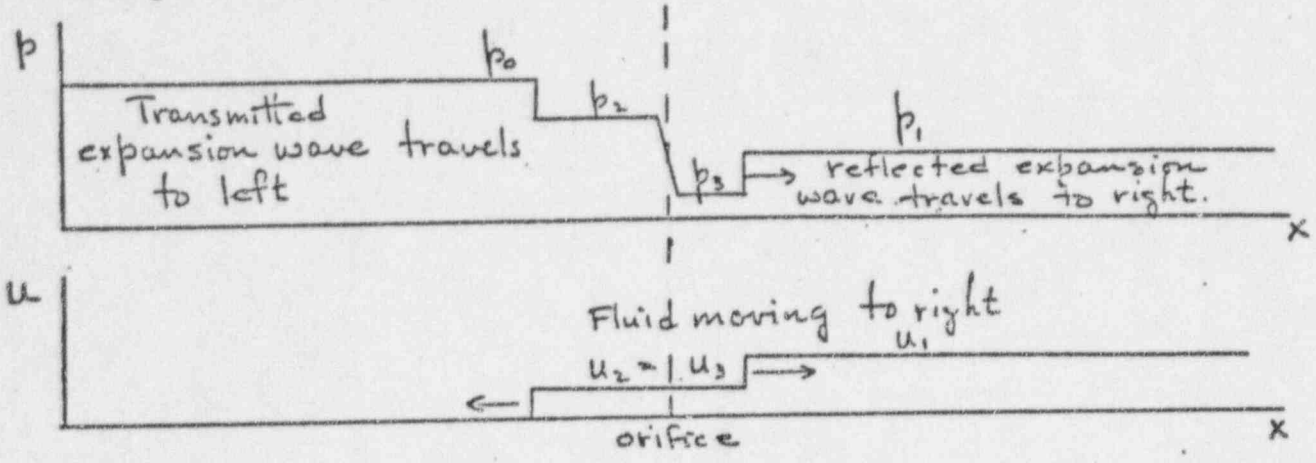

Figure A5

Note that the pressure is discontinuous because of the orifice pressure drop, but the velocity is continuous. We now have 2 waves, one transmitted <u>left</u> wave, one reflected <u>right</u> wave. Assuming as before $u \ll a$, we get:

For reflected wave:

$$p_3 - p_1 = \frac{\rho}{g} a (u_2 - u_1) \qquad \text{(A5)}$$

For transmitted wave:

$$p_0 - p_2 = \frac{\rho}{g} a (0 - u_2)(-1) = \frac{\rho}{g} a u_2 \qquad \text{(A6)}$$

The pressure drop across the orifice is

$$p_2 - p_3 = K \frac{\rho}{g} \frac{u_2^2}{2} \qquad \text{(A7)}$$

Adding (A5) and (A6), we get

$$(p_3 - p_2) + (p_0 - p_3) = 2 \frac{\rho}{g} a u_2 - \frac{\rho}{g} a u_1 \qquad \text{(A8)}$$

Substituting for u_2 from (A6) and u_1 from (A4), we obtain

$$2(p_0 - p_1) = 2(p_0 - p_2) + (p_3 - p_2)$$

or

$$p_0 - p_1 = (p_0 - p_2) + \tfrac{1}{2}(p_3 - p_2) \qquad \text{(A9)}$$

which says that the original pressure disturbance is equal to the transmitted disturbance plus one half the orifice drop. In terms of velocities, (A9) becomes

$$\frac{\rho}{g} a u_1 = \frac{\rho}{g} a u_2 + \frac{K}{4} \frac{\rho}{g} u_2^2$$

or

$$u_2^2 + \frac{4}{K} a u_2 - \frac{4}{K} a u_1 = 0$$

$$u_2 = \frac{-\frac{4a}{K} \pm \sqrt{\left(\frac{4a}{K}\right)^2 + \frac{16a}{K} u_1}}{2} \qquad \text{(A10)}$$

Obviously, we want the positive root.

$$u_2 = \frac{-\frac{4a}{K} + \frac{4a}{K}\sqrt{1 + \frac{K^2}{16a^2}\frac{16 a u_1}{K}}}{2}$$

$$u_2 = \frac{2a}{K}\left\{\sqrt{1 + \frac{K u_1}{a}} - 1\right\} \qquad \text{(A11)}$$

The key equations are thus:

$$p_1 - p_0 = -\frac{\rho}{g} a u_1 \qquad \text{(A12-a)}$$

$$u_2 = \frac{2a}{K}\left\{\sqrt{1+\frac{K u_1}{a}} \quad -1\right\} \qquad \text{(A12-b)}$$

$$p_3 - p_0 = p_1 - p_0 + \frac{\rho}{g} a (u_2 - u_1) \qquad \text{(A12-c)}$$

$$p_2 - p_0 = -\frac{\rho}{g} a u_2 \qquad \text{(A12-d)}$$

The above results are now applied to the following numerical example (the numbers are chosen to facilitate a later comparison with other results):

$$a = 2038 \text{ ft/sec.}$$
$$K = 576 \ *$$
$$u_1 = 20.3 \text{ ft/sec}$$
$$\rho/g = .048 \text{ slugs/ft}^3$$
$$p_0 = 144{,}531 \text{ psf.}$$

The so-called acoustic impedance is therefore

$$\frac{\rho}{g} a = 97.82$$

From equation (A12-a)

$$p_1 - p_0 = -(97.82)(20.3) = -1985.8 \text{ psf} = -13.8 \text{ psi}$$

---

*The losses in orifice flow come primarily from the sudden expansion on the downstream side. This value of K was therefore obtained from the analytical expression

$$K = \left(1 - \frac{A_1}{A_2}\right)$$

for a sudden expansion in incompressible flow (10).

Using (A12-b)

$$u_2 = \frac{(2)(2038)}{576}\left\{\sqrt{1+\frac{(576)(20.3)}{(2038)}} - 1\right\}$$

$$u_2 = 11.3 \text{ ft/sec.}$$

Using (A12-c)

$$p_3 - p_0 = -1985.8 + 97.82\,(11.3 - 20.3)$$

$$p_3 - p_0 = -2866.2 \text{ psf} = -19.9 \text{ psi}$$

Using (A12-d)

$$p_2 - p_0 = -(97.82)(11.3) = -1105.4 \text{ psf}$$

$$= -7.7 \text{ psi}$$

Reservoir Problem

The same analysis is now applied to the cases in which the upstream side of the orifice is a reservoir. Up to the time the wave hits the orifice, the situation is the same as above. After the wave hits the orifice, we have:

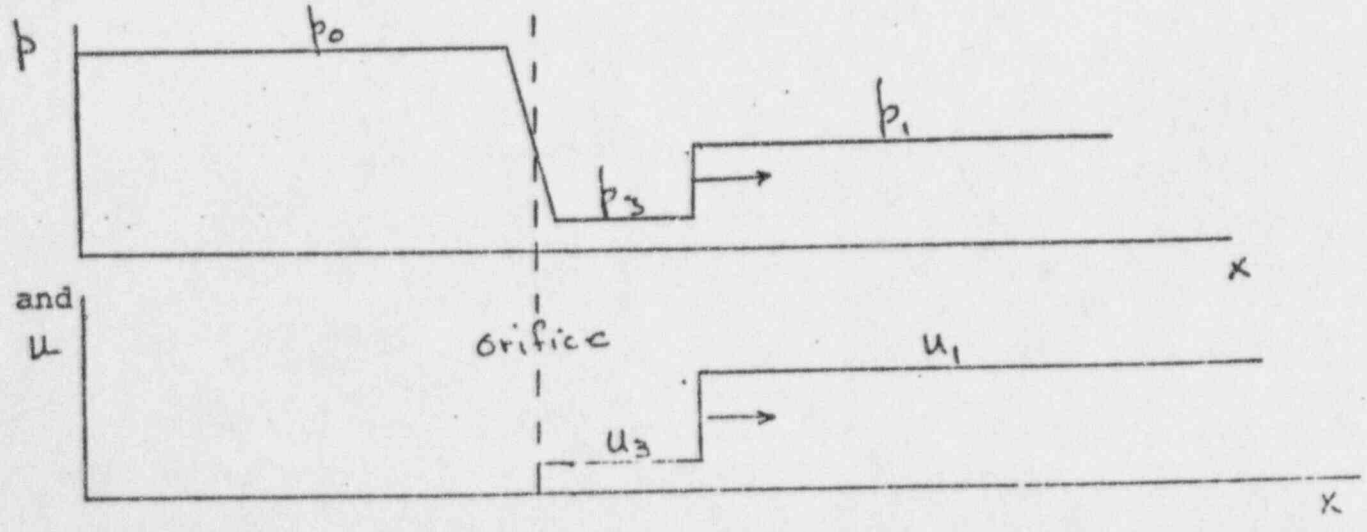

Figure A6

Thus, using (A1)

$$p_3 - p_1 = \frac{\rho}{g} a (u_3 - u_1) \qquad \text{(A13)}$$

and the orifice equation

$$p_0 - p_3 = K \frac{\rho}{g} \frac{u_3^2}{2} \qquad \text{(A14)}$$

but

$$p_3 - p_1 = (p_3 - p_0) + (p_0 - p_1) \qquad \text{(A15)}$$

and from (A12-a)

$$p_0 - p_1 = \frac{\rho}{g} a u_1 \qquad \text{(A16)}$$

Substituting,

$$\frac{\rho}{g} a (u_3 - u_1) = -K \frac{\rho}{g} \frac{u_3^2}{2} + \frac{\rho}{g} a u_1 \qquad \text{(A17)}$$

thus

$$K \frac{u_3^2}{2} + a u_3 - 2 a u_1 = 0$$

or

$$u_3^2 + \frac{2a}{K} u_3 - \frac{4a}{K} u_1 = 0 \qquad \text{(A18)}$$

with solution

$$u_3 = \frac{a}{K} \left\{ \sqrt{1 + \frac{4K}{a} u_1} - 1 \right\} \qquad \text{(A19)}$$

Thus the key equations for the reservoir case are

$$p_1 - p_0 = -\frac{\rho}{g} a u_1 \qquad \text{(A20-a)}$$

$$u_3 = \frac{a}{K}\left\{\sqrt{1+\frac{4K}{a}u_1} - 1\right\} \qquad \text{(A20-b)}$$

and

$$p_2 - p_0 = (p_1 - p_0) + \frac{\rho}{g} a (u_3 - u_1) \qquad \text{(A20-c)}$$

Numerical Example

Using the same data as before we obtain the following results.

$$p_1 - p_0 = -1985.8 \text{ psf}$$
$$= -13.8 \text{ psi}$$

$$u_3 = \frac{2038}{576}\left\{\sqrt{1+\frac{(4)(576)(20.3)}{(2038)}} - 1\right\}$$

$$u_3 = 13.78 \text{ ft/sec.}$$

$$p_3 - p_0 = -1985.8 + (97.82)(13.78 - 20.3)$$

$$p_3 - p_0 = -2623.9 \text{ psf}$$
$$= -18.2 \text{ psi}$$

The schematic below summarizes both cases for comparison.

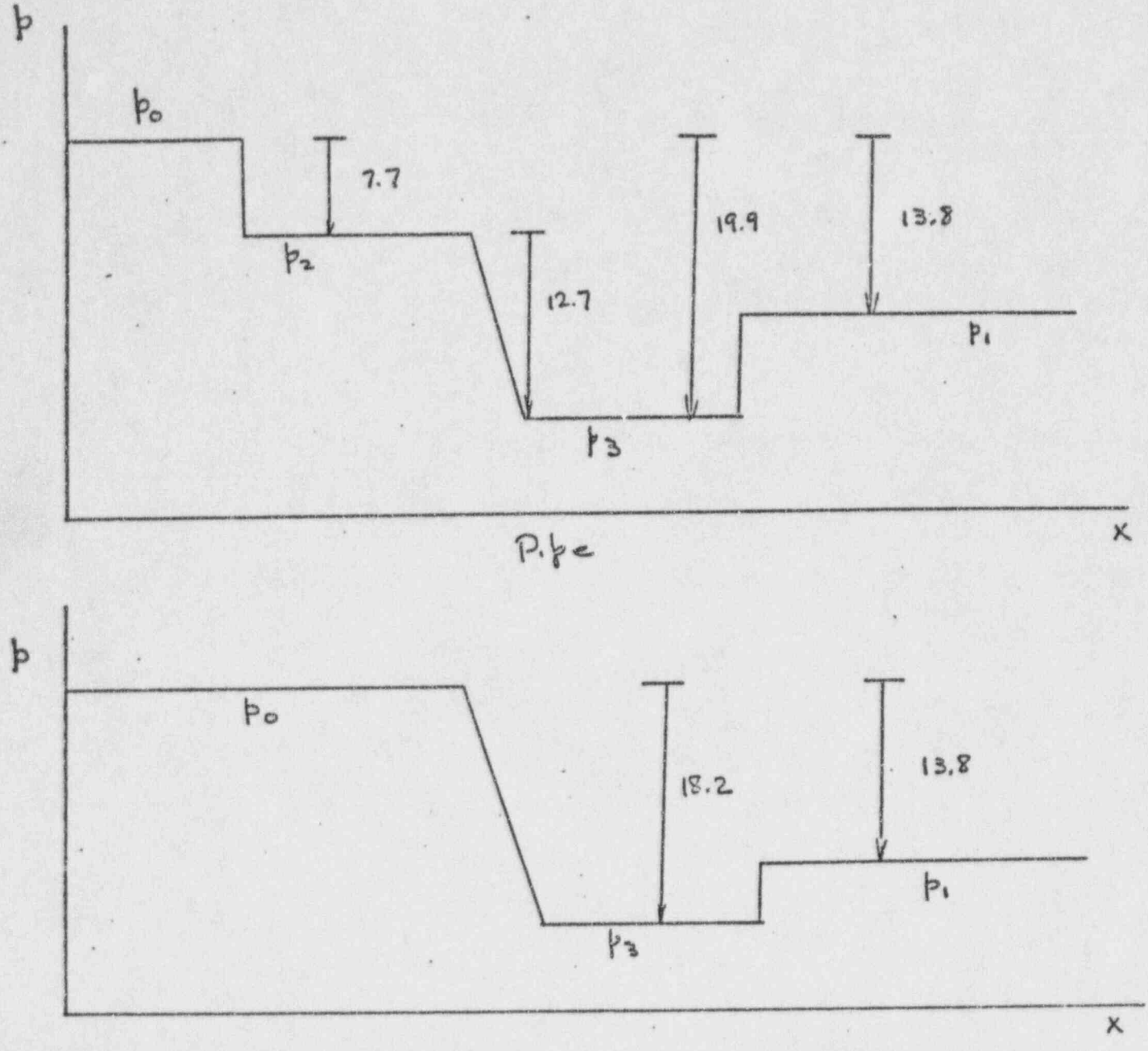

Figure A7

B. General Compressible Analysis

Use of the analysis in Section A in problems involving strong waves would no doubt lead to significant error. To provide for such cases the following analysis of unsteady compressible flow in a pipe or duct is also included. The bulk of the material presented is taken from the book on the subject by Rudinger (reference 4).

General Approach

In general, problems involving the propagation and interaction of finite amplitude waves in a compressible fluid are much too complicated to be treated analytically. Fortunately, the mathematical properties of the equations involved are particularly useful in constructing a finite difference scheme and this is the approach that has been chosen in this case. The basis for the technique is what is known as the theory of characteristics.

In the case of two independent variables the characteristics of the class of partial differential equations that frequently arise in fluid mechanics are curves in the plane of these variables. They can be identified by any of a number of properties, but from an operational point of view the most important one is that the dependent variables of the problem are related along each of these curves by an ordinary differential equation. The form of these relations and the expressions for the characteristic curves can be obtained from the governing equations. As a results of these properties the basic scheme can be simply explained in terms of the following example. In a one-dimensional, unsteady, isentropic flow problem the dependent variables are the velocity u and one thermodynamic variable. It is frequently very convenient

to use the sound speed a as this second variable. Through each point in the x-t plane would pass two characteristic curves of different slope. Along each of these curves u and a would be related through a known, ordinary differential equation. Now consider a point 3 a small distance away from a non-characteristic curve along which the solution is known. This curve can either be a boundary curve or one on which the values of u and a have been determined by previous calculation. The two characteristics are seen to provide a set of simultaneous equations for u_3 and a_3 in terms of u_1, u_2, a_1 and a_2. If the distances involved are sufficiently small the curves can be taken as straight lines and the equations can be written in simple difference form and solved algebraically.

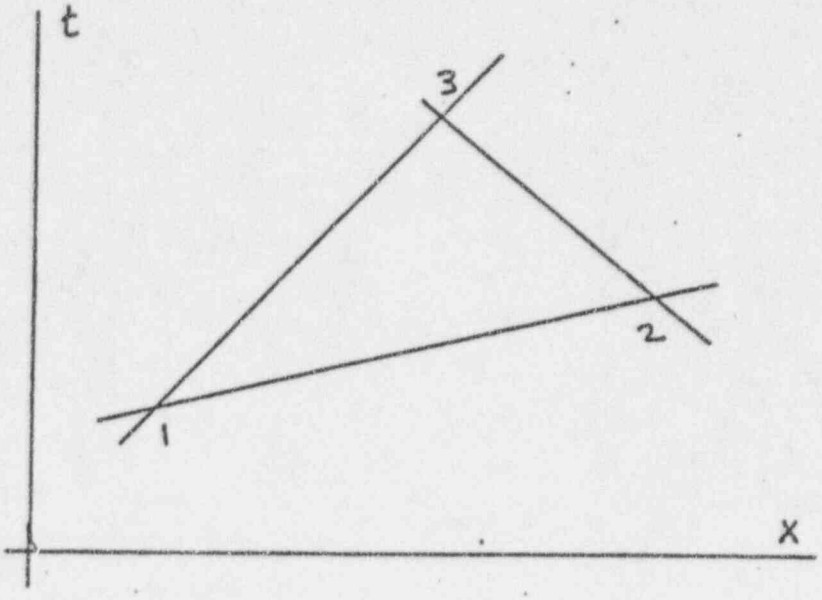

Figure B-1

In what follows the above approach will be applied to the problem of unsteady flow in a duct or pipe containing an orifice. The above general picture will thus be considerably filled in in the process. No attempt will be made to present the aspects of the theory of characteristics which lead to the steps taken. Such a complete development would be lengthy and is already available elsewhere. You are referred to any of references (5) through (7), with the first two being very similar and recommended. Xerox copies of these are appended to this report.

Basic Equations and Problem Formulation

The problem considered is the flow of a gas in a duct of uniform cross-section. At some point inside the duct there is an orifice. Initially the gas is at rest in the state determined by isentropically compressing it to a given pressure from atomospheric pressure (15.0 psia) and temperature (60 degrees F). At time zero the right end of the pipe is partially opened to the atmosphere. The force on the orifice due to the resulting expansion is to be determined.

The gas will be assumed to be perfect. In addition the diameter of the pipe is assumed to be sufficiently small in relation to its length that the flow can be treated as one dimensional. The flow is taken to be adiabatic and it is assumed that the losses in the orifice are sufficiently larger than frictional effects that the latter can be neglected. Under these circumstances the equations of conservation of mass and momentum can be written as

$$\frac{\partial \rho}{\partial t} + \frac{\partial \rho u}{\partial x} = 0 \qquad \text{(B1)}$$

and

$$\frac{\partial u}{\partial t} + u \frac{\partial u}{\partial x} = -\frac{1}{\rho} \frac{\partial p}{\partial x} \qquad \text{(B2)}$$

respectively. p and ρ are the pressure and density and u is the fluid velocity. The thermodynamic variables are related by the equation of state

$$p = \rho R T \qquad \text{(B3-a)}$$

where R is the gas constant and T the temperature. Since the sound speed will be used as one of our independent thermodynamic variables we will also have cause to use an alternative form of (B3-a). Sound speed is defined as

$$a^2 = (\partial p/\partial \rho)_s$$

where S is the entropy. Since if s is constant p and ρ are related by

$$p/\rho^\gamma = \text{constant}$$

where γ is the ratio of specific heats c_p/c_v, we have

$$a^2 = \gamma \frac{p}{\rho} = \gamma R T \qquad \text{(B3-b)}$$

The fourth equation is required to close this set and the most convenient choice involves the entropy. For the portion of the flow away from the orifice this will simply be

$$\frac{Ds}{Dt} = 0 \qquad \text{(B4)}$$

where the standard operator notation

$$\frac{D}{Dt} = \frac{\partial}{\partial t} + u \frac{\partial}{\partial x}$$

has been used. As explained below the orifice is to be treated in a manner different from the main flow. Although equation (B4) applies everywhere else the necessity to patch the two analysis together requires that the entropy be kept explicit in the formulation.

The most convenient set of variables for the problem turn out to be u, a and S. Equations (B1) and (B2) are therefore now put in that form. The results are then manipulated to obtain the form appropriate to analysis using characteristics. While the background has not been presented it is clear that if these equations are to be trasnformed into ordinary differential equations valid

shown here will have to combine to form derivatives along certain curves the derivatives in the direction of these curves. It is this end that motivates the following operations.

First the pressure and density can be eliminated from (B1) and (B2) in favor of a and s by use of the following thermodynamic relations valid for a perfect gas with constant specific heats.

$$ds = c_p \, d\ln T - \frac{R}{gJ} \, d\ln p$$

$$ds = c_v \, d\ln T - \frac{R}{gJ} \ln \rho$$

Using the relation

$$c_p - c_v = R$$

and the equation of state in the form

$$a^2 = \gamma R T$$

These equations can be written as

$$d\ln p = \frac{2\gamma}{\gamma-1} \, d\ln a - \frac{gJ}{R} \, ds$$

$$d\ln \rho = \frac{2}{\gamma-1} \, d\ln a - \frac{gJ}{R} \, ds \qquad \text{(B5)}$$

Similarly equations (B1) and (B2) can be conveniently changed to

$$\frac{\partial \ln \rho}{\partial t} + u \frac{\partial \ln p}{\partial x} + \frac{\partial u}{\partial x} = 0$$

$$\frac{\partial u}{\partial t} + u \frac{\partial u}{\partial x} = -\frac{a^2}{\gamma} \frac{\partial \ln p}{\partial x} \qquad \text{(B6)}$$

Thus, in terms of a, u and s, the continuity and momentum equations become

$$\frac{2}{\gamma-1} \frac{\partial a}{\partial t} + \frac{2}{\gamma-1} u \frac{\partial a}{\partial x} + a \frac{\partial u}{\partial x} = a \frac{gJ}{R} \frac{Ds}{Dt} \qquad \text{(B7)}$$

and

$$\frac{\partial u}{\partial t} + u\frac{\partial u}{\partial x} + \frac{2}{\gamma-1} a \frac{\partial a}{\partial x} = a^2 \frac{gJ}{\gamma R} \frac{\partial s}{\partial x} \qquad \text{(B8)}$$

The desired combination of derivatives mentioned above can now be obtained simply by alternatively adding and subtracting equation (B8) and equation (B7). The result is

$$\frac{d}{\partial t}\left(\frac{2}{\gamma-1} a \pm u\right) + (u \pm a)\frac{\partial}{\partial x}\left(\frac{2}{\gamma-1} a \pm u\right)$$

$$= a\frac{gJ}{R}\left(\frac{Ds}{Dt} \pm \frac{a}{\gamma}\frac{\partial s}{\partial x}\right) \qquad \text{(B9)}$$

The left hand side of this equation represents the derivatives of the variables $\frac{2}{\gamma-1} a \pm u$ in the directions given by

$$\frac{dx}{dt} = u \pm a$$

It is convenient to define

$$P = \frac{2}{\gamma-1} a + u \qquad Q = \frac{2}{\gamma-1} a - u$$

and also to introduce the operator notation

$$\frac{\delta_+}{\delta t} = \frac{\partial}{\partial t} + (u+a)\frac{\partial}{\partial x}$$

$$\frac{\delta_-}{\delta t} = \frac{\partial}{\partial t} + (u-a)\frac{\partial}{\partial x}$$

Thus (B9) becomes

$$\frac{\delta_+ P}{\delta t} = a \frac{gJ}{R}\left(\frac{Ds}{Dt} + \frac{a}{\gamma}\frac{\partial s}{\partial x}\right)$$

$$\frac{\delta_- Q}{\delta t} = a \frac{gJ}{R}\left(\frac{Ds}{Dt} - \frac{a}{\gamma}\frac{\partial s}{\partial x}\right).$$

Since

$$\frac{\partial}{\partial x} = \frac{\delta_+}{\delta t} - \frac{D}{Dt} = -\frac{\delta_-}{\delta t} + \frac{D}{Dt}$$

the notation can be made consistent. Thus

$$\frac{\delta_+ P}{\delta t} = a \frac{gJ}{\gamma R}\frac{\delta_+ s}{\delta t} + (\gamma-1)\, a \frac{gJ}{\gamma R}\frac{Ds}{Dt} \qquad \text{(B10)}$$

$$\frac{\delta_- Q}{\delta t} = a \frac{gJ}{\gamma R}\frac{\delta_- s}{\delta t} + (\gamma-1)\, a \frac{gJ}{\gamma R}\frac{Ds}{Dt} \qquad \text{(B11)}$$

It should be emphasized that equation (B10) is valid along the curve whose slope at every point is

$$\frac{dx}{dt} = u+a$$

while (B11) holds along curves specified by

$$\frac{dx}{dt} = u-a$$

We now non-dimensionalize all velocities by dividing by the speed of sound at atmospheric conditions. Similarly the entropy divided by $\gamma R/gJ$ is our non-dimensional entropy. Non-dimensional distance and time, defined by

$$\xi = \frac{x}{L}$$

$$\tau = \frac{a_a t}{L} = \frac{t}{t_a}$$

where a_a is the atmospheric sound speed and L a convenient length, are also introduced. For the present problem L is taken to be the distance from the end of the duct to the orifice. Equations (B10) and (B11) thus become

$$\frac{\delta_+ P}{\delta \tau} = a \frac{\delta_+ S}{\delta \tau} + a(\gamma - 1) \frac{DS}{D\tau} \qquad \text{(B12)}$$

$$\frac{\delta_- Q}{\delta \tau} = a \frac{\delta_- S}{\delta \tau} + a(\gamma - 1) \frac{DS}{D\tau} \qquad \text{(B13)}$$

The system of equations is formally ~~completed~~ completed by adding the generalization of equation (B4). This could be written as

$$\frac{DS}{D\tau} = F(a, u, s, \xi, \tau) \qquad \text{(B*)}$$

The function F would have to be specified for particular problems depending on the nature of the heating, combustion or other appropriate irreversibility. As will be seen shortly it will not be necessary to deal explicitly with F in the present case.

Since equations (B12), (B13) and (B14) indicate how the variables P, Q and S vary along the curves

$$\frac{d\xi}{d\tau} = u + a$$

$$\frac{d\xi}{d\tau} = u - a$$

and $$\frac{d\xi}{d\tau} = u$$

respectively, the formulation of the problem in characteristic terms is complete.

Before continuing with the specific problem at hand it may be worthwhile to return to the case of isentropic flow used earlier as an example. The pertinent equations and curves can now be made explicit. Since a significant portion of the flow is isentropic the results for that case will be doubly useful.

In this case equation (B14) is no longer necessary and equations (B12) and (B13) reduce to

$$P = \frac{2}{\gamma-1} a + u = \text{constant along } \frac{d\xi}{d\tau} = u + a ,$$

and

$$Q = \frac{2}{\gamma-1} a - u = \text{constant along } \frac{d\xi}{d\tau} = u - a .$$

The solution at point 3 in the sketch shown in terms of the properties at points 1 and 2 is thus quite simple. The characteristic form 1 to 3 has the positive slope so the solution would be

$$a_3 = \frac{\gamma-1}{4}(P_1 + Q_2) \qquad \text{(B15)}$$

$$u_3 = \frac{1}{2}(P_1 - Q_2) \qquad \text{(B16)}$$

Using a different scale it is easy to see how grid covering an entire flow field can be mapped out by repeatedly applying the above scheme. In addition to point 3, point 5 can be determined from

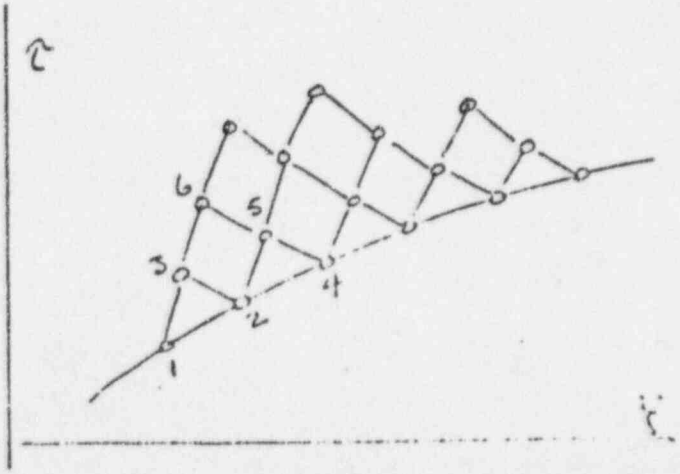

Figure B2

2 and 4. The results of these two calculations lead to the solution at 6 and so forth. It is pertinent to note for what follows that in the isentropic case P (or Q as the case may be) is constant along a particular curve. In general the value of P will vary from one member to another of the family of characteristics with positive slope. In addition the values of u and a will usually vary along any given curve. This is because any given P -curve will be intersecting Q -curves of changing value. The value of $\frac{2}{\gamma-1}a+u$ (or $\frac{2}{\gamma-1}a-u$) remains constant along any given P (or Q) curve however.

Resevoir Problem

In the problem under consideration here the area to be mapped in is $0 \le \xi \le 1$, $\hat{t} \ge 0$. At $\hat{t}=0$ the gas is at rest at the given initial temperature. The value of P or Q along any characteristic that terminates at any point on the $\hat{t}=0$ line is therefore known:

$$P = \frac{2}{\gamma-1} a_0 = Q$$

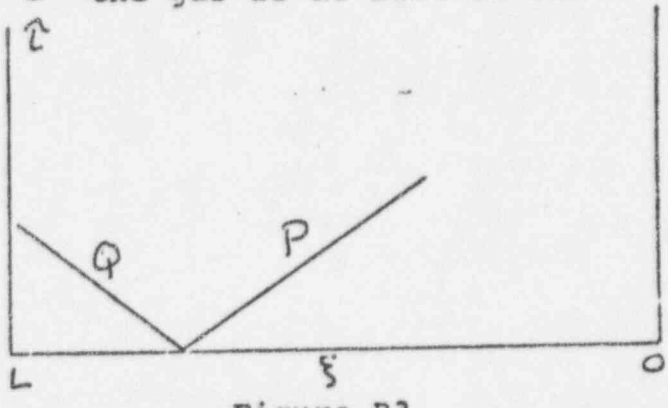

Figure B3

where a_0 is the sound speed in the initial, undisturbed state of the gas. The flow is assumed to be initiated by instantaneously opening the end at $\xi = 0$ to the atmosphere (the orifice is located at $\xi = L$) causing the gas at that point to immediately take on a finite velocity. The value of that velocity depends on the detailed boundary condition imposed and will be discussed below. As a result

an entire family of Q -characteristics emanate from the $\xi=0,\ \tau=0$ point, one for each value of the velocity between zero and the maximum imposed by the boundary condition. Such a fan is called a "centered expansion wave". The bottom-most Q curve represents the leading edge of the wave. The value of Q along with curve is thus $\frac{2}{\gamma-1} a_0$. The topmost Q curve represents the trailing edge of the wave. The fluid velocity there is the maximum caused by the wave, call it u_{max} for the present. It's value, again, is determined by the boundary condition. The value of Q along this top-most curve is determined from this known u_{max} and the fact that the value of any intersecting P - characteristic orginating on the $\tau=0$ line is known. Designating an arbitrary point on this cruve by α we have

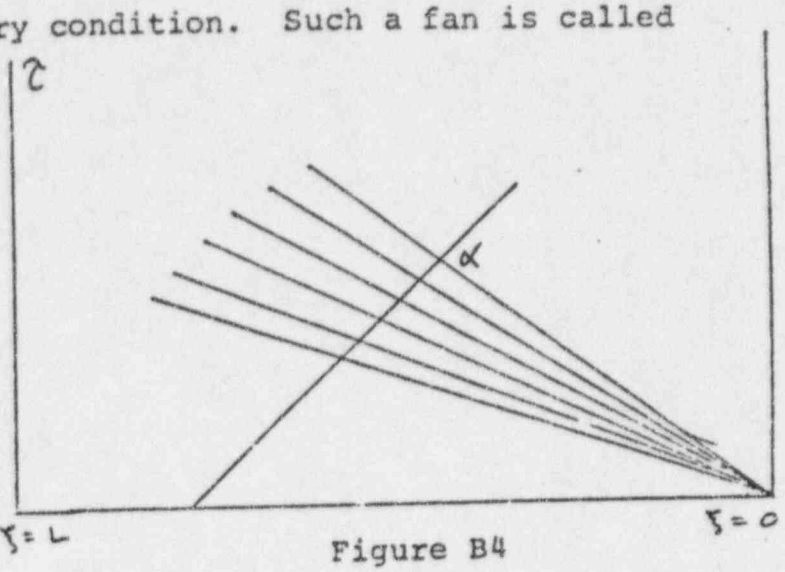

Figure B4

$$P_\alpha = \frac{2}{\gamma-1} a_\alpha + u_\alpha = \frac{2}{\gamma-1} a_0$$

But $u_\alpha = u_{max}$, therefore

$$a_\alpha = a_0 - \frac{\gamma-1}{2} u_{max}$$

and

$$Q_\alpha = \frac{2}{\gamma-1}\left\{ a_0 - \frac{\gamma-1}{2} u_{max} \right\} - u_{max}$$

$$Q_\alpha = \frac{2}{\gamma-1} a_0 - 2 u_{max}$$

The slope of the Q - characteristic at α is also known

$$\left.\frac{d\xi}{d\tau}\right|_{Q@\alpha} = u_{max} - a_\alpha \quad .$$

The values of Q for the other characteristics of the expansion fan, as well as their slopes, can be determined similarly.

The characterestistics thus clearly show the propagation of the wave. As it moves down the pipe it spreads since the elements of the expansion progressively lower the temperature of the gas and hence the sound speed behind them. The profile of the wave at any time such as those indicated by the dotted lines is given by the values of u and a, and hence p, ρ, etc. at the points of intersection of the characteristics and the $\tau = c$ line. Although there are two characteristics through each point in the plane only those which delineate regions of change are plotted.

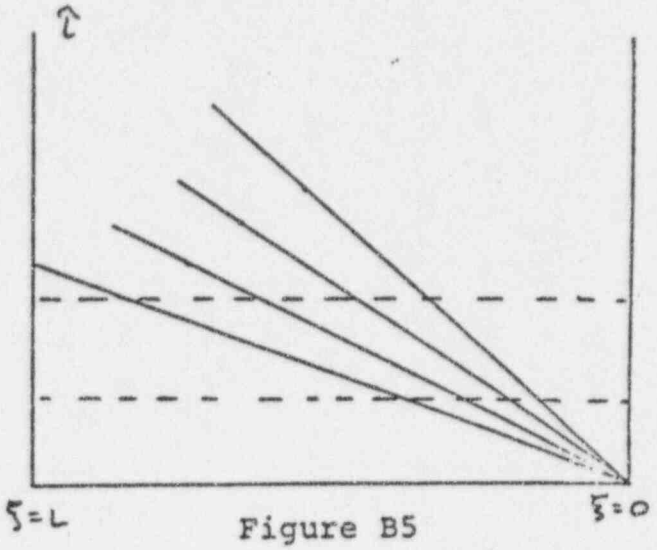

Figure B5

The above conditions apply until the leading edge of the wave strikes the wall containing the orifice. The two characteristics through this point are shown in Figure 6. It is seen that the Q-characteristic is reflected as a P- characteristic at the orifice. The details of the reflection process are again to be determined from the boundary conditions. In the simplest case of a solid wall this

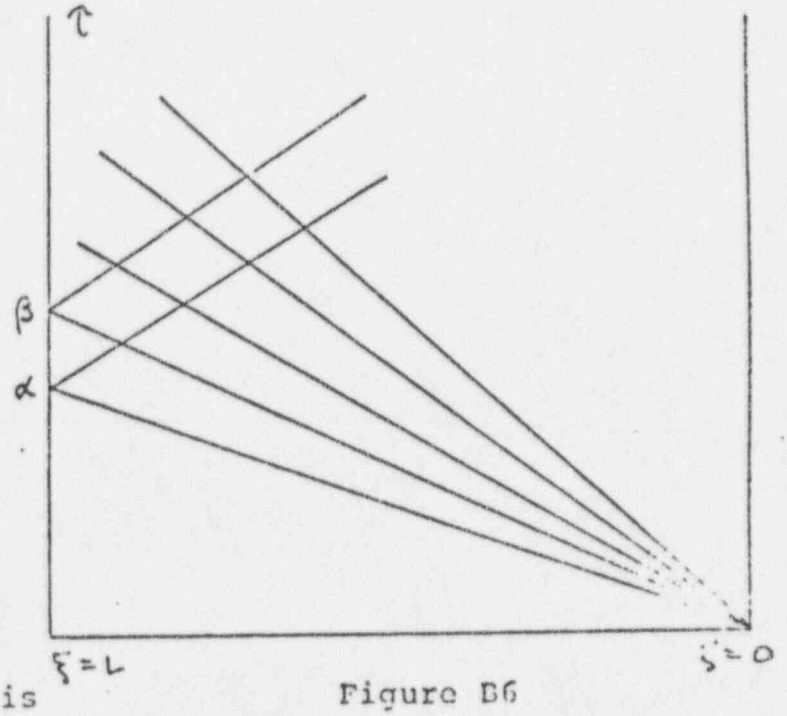

Figure B6

would be $u_L \sim 0$. Thus, again designating the point in question by α we have by equations (B15) and (B16).

$$P_\alpha = Q_\alpha$$

and

$$a_\alpha = \frac{\gamma-1}{4}\left(P_\alpha + Q_\alpha\right)$$

Since Q_α is now known P_α and a_α can be determined. Similarly when the second characteristic hits the wall at β

$$P_\beta \sim Q_\beta \quad (\neq Q_\alpha)$$

$$a_\beta = \frac{\gamma-1}{4}\left(P_\beta + Q_\beta\right)$$

If the parition at $\xi = L$ contains an orifice the situation is considerably more complicated. First of all the boundary condition is not so simply stated. The velocity is not zero. The incident expansion wave will induce a finite fluid velocity through the orifice. Only part of the incident wave will be reflected while part will be transmitted through the opening. Secondly, the value of Q on the incoming characteristic is no longer known. This is because the flow through the orifice is not isentropic and this results in a change of Q as the orifice is approached as shown by equation (B13). The detailed formulation of the boundary condition at the orifice will be taken up shortly. The important point now is that the properties of the reflected wave are determined from appropriate boundary conditions. In the procedure itself the amount of reflection and transmission and all other aspects of the interaction with the wall are distilled into the value of the characteristic variable P which leaves the point in question.

From this point on the wave diagram gets increasingly more complicated as a complex pattern of reflections and interactions builds up in time.

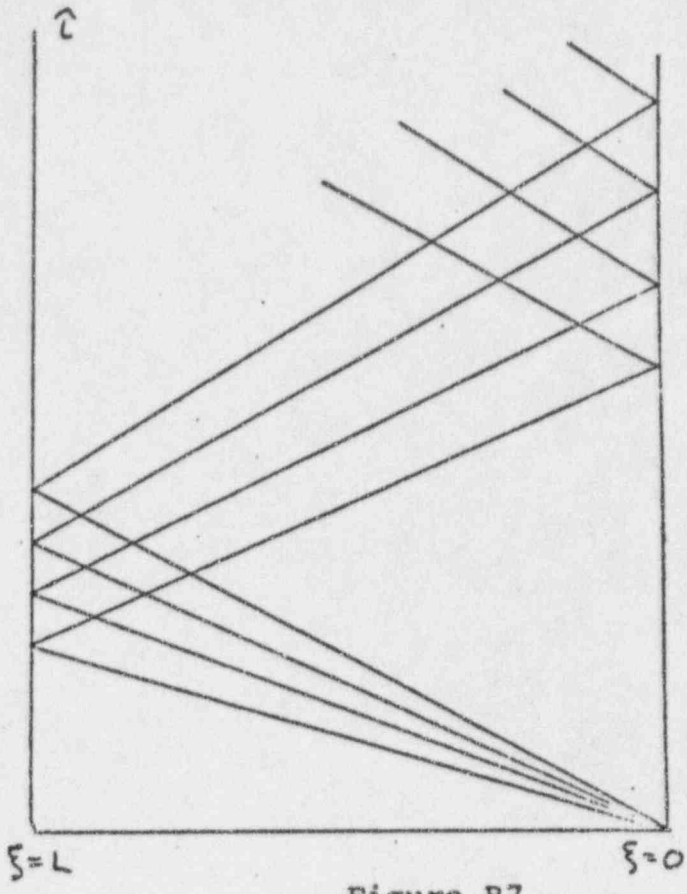

Figure B7

If the upstream side of the orifice acts as a reservoir conditions there are of course known. If the pipe continues however the unsteady flow in that region can be determined in a similar manner. The boundary condition consistent with the effects of the incident wave is determined and the calculation is begun as before. In this instance however the fluid is accelerated at a finite rate and the result is not a centered expansion wave. This means that the C_+ -characteristics comprising the expansion will not originate at a common point but will be distributed along that short segment of the time axis subtended by the incident wave.

Boundary Conditions

The opening to the atmosphere at the right-hand end of the pipe is treated as a short, isentropic nozzle. The assumption is based on the fact that the fluids in the corners will be essentially stagnant. The flow pattern does not have the turbulent secondary

flows that normally characterize a region of significant losses. An effective exit area which accounts for the usual over-contraction of the flow should be used in what follows however.

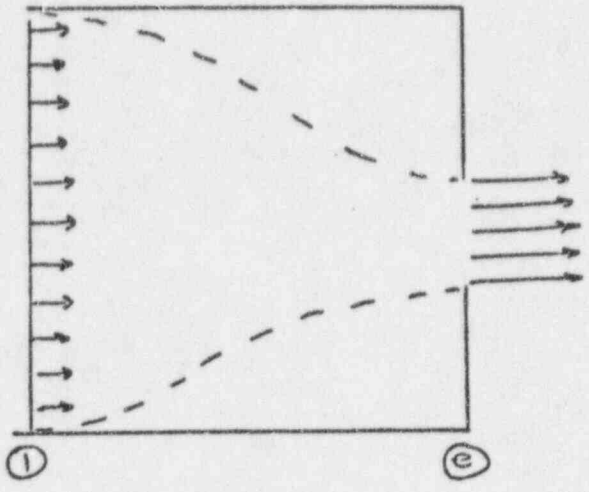

Figure B8

Since we take the fluid at position one to be accelerated instantaneously when the opening at e occurs the flow in the nozzle is computed assuming steady state prevails. The pressure in the ambient gas is assumed known. As long as the flow is subsonic the appropriate boundary condition at e is $p_e = p_{ambient}$. When the flow becomes choked this condition becomes

$$M_e = \frac{u_e}{a_e} = 1$$

where M is the Mach number.

From either p_e or M_e and the area ratio A_1/A_e the conditions at position 1 can be determined from the equations of one-dimensional isentropic flow. If the flow is choked the M_1 can be determined from

$$\frac{A_1}{A_e} = \frac{1}{M_1}\left\{\left(\frac{2}{\gamma+1}\right)\left(1+\frac{\gamma-1}{2}M_1^2\right)\right\}^{\frac{\gamma+1}{2(\gamma-1)}}$$

If, on the other hand, p_e is known M_1 is determined from

$$\frac{A_1}{A_e}\frac{p_o}{p_e}\left(\frac{2}{\gamma+1}\right)^{1/2} = \frac{1}{M_1}\left\{1+\frac{\gamma-1}{2}M_1^2\right\}^{\frac{\gamma+1}{2(\gamma-1)}}$$

where p_0 is the initial pressure in the pipe. These equations can be derived from the basic conservation laws and are developed (although in a slightly different form) in, for example, Shapiro (3). The obvious algebraic complexity of these equations can be avoided by using the gas tables such as those in Shapiro or Keenan and Kaye (8). The relations between the various dependent variables in one-dimensional isentropic flow are tabulated there. The equations can also be usefully plotted.

The treatment of the flow through the orifice is analogous to that just described for the opening at the end of the pipe. Flow on the upstream side of the orifice is again taken to be adequately modeled by a short isentropic nozzle. Except for the use of an effective orifice opening to allow for an over-contraction of the converging stream the losses in the orifice occur in the sudden expansion that occurs on the downstream side. The flow is again assumed to be steady. This implies that conditions at Section 1 adjust instantaneously to changes at Section 3. The flow between sections 2 and 3 is not treated in detail. Instead a balance of mass, momentum and energy is imposed along with the requirement that the flow at 1 and 3 be one-dimensional. Such a spontaneous change will involve an entropy increase and the solution will

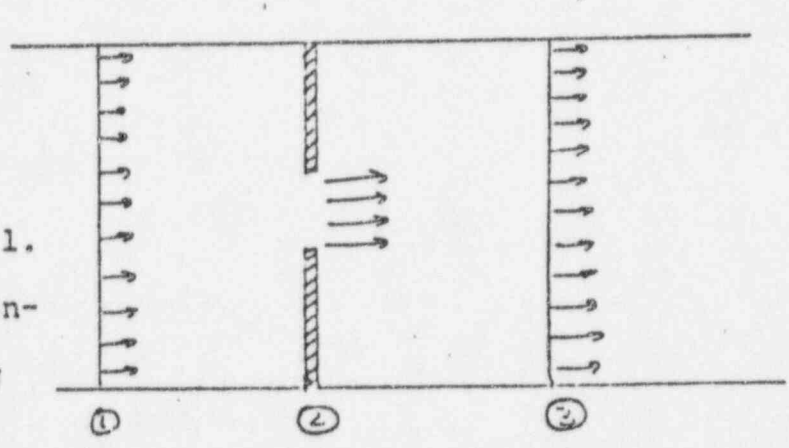

Figure B9

reflect this. A key assumption in this analysis is that the pressure on the downstream side of the orifice at Section 2 is equal to the pressure at the centerline of the flow. This assumption has been verified experimentally for all subsonic flows (9).

The equations available to determine the conditions at Section 3 are the following. At Section 3 we have the incident characteristic function

$$Q = \frac{2}{\gamma-1} a_3 - u_3 \qquad \text{(B17)}$$

The conditions at 1 and 3 can also be related by the steady flow energy equation

$$h_1 + \frac{u_1^2}{2} = h_3 + \frac{u_3^2}{2}$$

where h is the specific enthalpy of the fluid. Since for a perfect gas

$$h = c_p T + \text{constant}$$

and

$$R = c_p - c_v$$

use of equation (B36) leads to

$$h = \frac{a^2}{\gamma-1}$$

Thus the energy equation can be written in terms convenient to this analysis in the form

$$a_1^2 + \frac{\gamma-1}{2} u_1^2 = a_3^2 + \frac{\gamma-1}{2} u_3^2$$

In the case of an upstream reservoir $u_1 = 0$ and $a_1 = a_o$ the sound speed in the undisturbed gas. Since this case is somewhat simpler it will be used to demonstrate the method. The pipe problem can be treated similarly but involves additional algebraic complications. We thus write

$$a_o^2 = a_3^2 + \frac{\gamma-1}{2} u_3^2 \qquad \text{(B18)}$$

Conservation of mass, momentum and energy between sections 2 and 3 imply

$$\rho_2 u_2 A_2 = \rho_3 u_3 A_3 \qquad \text{(B19)}$$

$$p_2 A_3 + \rho_2 u_2^2 A_2 = p_3 A_3 + \rho_3 u_3^2 A_3 \qquad \text{(B20)}$$

and

$$a_2^2 + \frac{\gamma-1}{2} u_2^2 = a_3^2 + \frac{\gamma-1}{2} u_3^2 \qquad \text{(B21)}$$

The final equation required to close this set comes from specifying that the flow to point 2 is isentropic.

$$s_2 = s_1 = s_o$$

But since the gas was initially compressed isentropically from the ambient state $s_o = s_a$. Furthermore, we are free to assign the value of s_a arbitrarily since only entropy differences are of significance. We thus obtain

$$s_2 = 0$$

The most useful form of this condition however comes from the first of equations (B5). Putting it in non-dimensional form and integrating between the ambient state and state 2 yields:

$$\gamma(s_2 - s_a) = \frac{2\gamma}{\gamma-1} \ln a_2 - \ln p_2$$

Therefore

$$p_2 = (a_2)^{\frac{2\gamma}{\gamma-1}} \qquad \text{(B22)}$$

The above entropy equation written between 2 and 3 will also be useful in the following form

$$s_3 = \frac{1}{\gamma-1} \ln \frac{a_3^2}{a_2^2} - \frac{1}{\gamma} \ln \frac{p_3}{p_2} \qquad \text{(B23)}$$

Equations (B17) -- (B22) plus the pair

$$a_2^2 = \gamma \frac{p_2}{\rho_2} \qquad \text{and} \qquad a_3^2 = \gamma \frac{p_3}{\rho_3}$$

provide eight equations for the eight unknown variables $u_2, a_2, p_2, p_2, u_3, a_3, \rho_3$ & p_3 provided Q is known. As mentioned earlier however this is not the case. Thus the use of an iteration procedure is indicated. A value of Q is assumed and the other variables calculated. Q is then calculated from equation (B23). A new value of Q is then computed from equation (B13) written between the orifice wall and a previously calculated point on the Q -characteristic leading to the wall such as point β in

$$1+\gamma\frac{A_2}{A_3}M_2^2=\frac{p_3}{p_2}\left(1+\gamma M_3^2\right) \qquad \text{(B27)}$$

and

$$\frac{a_2^2}{a_3^2}\left\{1+\frac{\gamma-1}{2}M_2^2\right\}=1+\frac{\gamma-1}{2}M_3^2 \qquad \text{(B28)}$$

respectively. (B26) and (B27) are now combined to obtain

$$\left\{\gamma\frac{A_3}{A_2}\left(\frac{a_2}{a_3}\right)^2M_3^2\right\}\left(\frac{p_3}{p_2}\right)^2-\left\{1+\gamma M_3^2\right\}\frac{p_3}{p_2}+1=0$$

Similarly (B26) and (B28) yield

$$\left\{\frac{\gamma-1}{2}\left(\frac{p_2}{p_2}\frac{A_3}{A_2}M_3\right)^2\right\}\left(\frac{a_2^2}{a_3^2}\right)^2+\frac{a_2^2}{a_3^2}-\left\{1+\frac{\gamma-1}{2}M_3^2\right\}=0$$

These are two coupled quadratics in the ratios p_3/p_2 and a_2^2/a_3^2 in terms of M_3 which has already been obtained. The utility of this formulation comes in when computing S_3 from equation (B23). In the general case an iterative or graphical solution would be required. A series solution valid for small M_3 can be obtained analytically however.

The formal solutions to these equations are

$$\frac{a_2^2}{a_3^2}=\frac{-1+\sqrt{1+4\left\{\frac{\gamma-1}{2}\left(\frac{p_3}{p_2}\frac{A_3}{A_2}M_3\right)^2\right\}\left\{1+\frac{\gamma-1}{2}M_3^2\right\}}}{2\left\{\frac{\gamma-1}{2}\left(\frac{p_3}{p_2}\frac{A_3}{A_2}M_3\right)^2\right\}}$$

and

$$\frac{p_3}{p_2}=\frac{1+\gamma M_3^2-\sqrt{\left(1+\gamma M_3^2\right)^2-4\left\{\gamma\frac{A_3}{A_2}\left(\frac{a_2}{a_3}\right)^2M_3^4\right\}}}{2\left\{\gamma\frac{A_3}{A_2}\left(\frac{a_2}{a_3}\right)^2M_3^2\right\}}$$

Figure B10. If the iteration is being used to determine the conditions at α. Since the flow between α and β is isentropic

$$\frac{Ds}{Dt} = 0$$

and we can write

$$Q_\alpha - Q_\beta = a\,(s_\alpha - s_\beta)$$

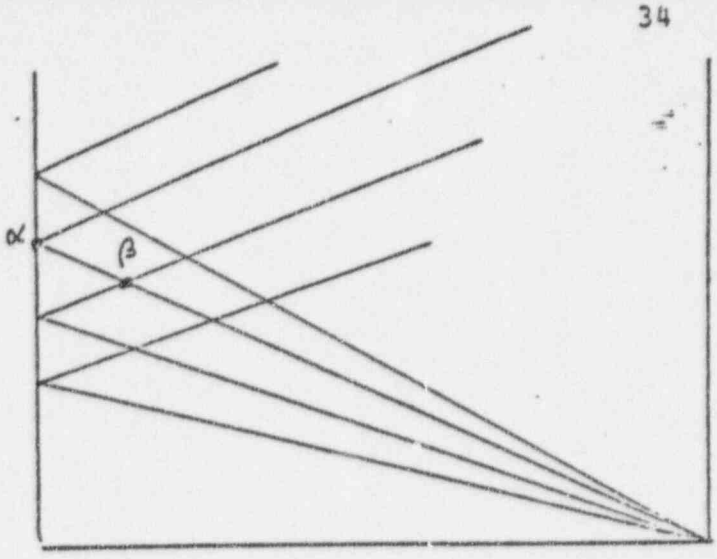

Figure B10

Unless the fluid flowing from the orifice has reached β, $s_\beta = 0$. Thus

$$Q_\alpha = Q_\beta + \left(\frac{a_\alpha + a_\beta}{2}\right) s_\alpha \qquad \text{(B24)}$$

where an average a has been used.

To actually obtain a solution the following manipulations are useful, especially for low Mach numbers at point 3. Equations (B17) and (B18) can be solved for a_3 in terms of Q and a_0

$$a_3 = \frac{Q \pm \sqrt{\frac{\gamma+1}{\gamma-1} a_0^2 - \frac{\gamma-1}{2} Q^2}}{\frac{\gamma+1}{\gamma-1}} \qquad \text{(B25)}$$

The "minus" solution corresponds to supersonic flow in the expansion and is discarded. The velocity u_3, and hence M_3, can then be obtained from (17). Equations (B19), (B20) and (B21) are then rearranged with the help of the two equations of state to obtain

$$M_2 = \frac{p_3}{p_2} \frac{A_3}{A_2} \frac{a_2}{a_3} M_3 \qquad \text{(B26)}$$

where only the appropriate sign of the radical has chosen. If these radicals are now expanded by the binomial theorem we obtain

$$\frac{a_2^2}{a_3^2} = 1 + \frac{\gamma-1}{2} M_3^2 \left\{ 1 - \left(\frac{p_3}{p_2}\right)^2 \left(\frac{A_3}{A_2}\right)^2 \right\} - 2 \left(\frac{\gamma-1}{2} \frac{p_3}{p_2} \frac{A_3}{A_2} M_3^2 \right)^2 \left(1 - \left(\frac{p_3}{p_2} \frac{A_3}{A_2}\right)^2 \right)$$

$$\frac{p_3}{p_2} = 1 + \gamma M_3^2 \left\{ \frac{A_3}{A_2} \left(\frac{a_2}{a_3}\right)^2 - 1 \right\} - \gamma^2 M_3^4 \left\{ 3 \frac{A_3}{A_2} \left(\frac{a_2}{a_3}\right)^2 - 1 \right\}$$

Substituting one into the other, solving the resulting quadratic and expanding again leads to

$$\frac{p_3}{p_2} = 1 + \gamma \left(\frac{A_3}{A_2} - 1 \right) M_3^2 - \gamma \left(\frac{\gamma-1}{2} \right) \frac{A_3}{A_2} \left\{ \left(\frac{A_3}{A_2}\right)^2 - 1 \right\} M_3^4 + O(M^6) \quad \text{(B29)}$$

$$\frac{a_2^2}{a_3^2} = 1 + \frac{\gamma-1}{2} \left(1 - \frac{A_3^2}{A_2^2} \right) M_3^2 - 2 \left(\frac{\gamma-1}{2} \right)^2 \left(\frac{A_3}{A_2} \right)^2 \left\{ 1 - \left(\frac{A_3}{A_2} \right)^2 \right\} M_3^4 + O(M^6) \quad \text{(B30)}$$

For low M_3 the iteration scheme is simply:

1. Assume Φ
2. compute a_3 from (B25)
3. compute u_3 from (B17)
4. compute M_3.
5. compute p_3/p_2 and a_2^2/a_3^2 from above.
6. compute S from (B23)
7. compute a new Φ from (B24)

Calculation of conditions at the orifice is now complete. The P -characteristic at the wall point say α in Figure 10, is known from

$$P = \frac{2}{\gamma-1} a_\alpha + u_\alpha$$

The calculation can be continued to point β by calculation of the value of P_β at that point from equation (B12). Again $Ds/Dt = 0$ so that

$$P_\beta = P_\alpha - a_\alpha S_\alpha$$

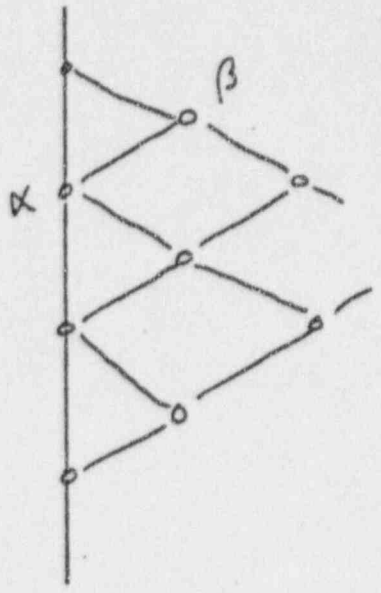

Figure B11

Numerical Example.

The following numerical example will serve to further clarify the above procedure as well as to verify that the water-hammer analysis is quite adequate for waves of small amplitude.

Ambient conditions are again taken to be 15 psia and 60 degrees F. For simplicity the calculation is made for air with a γ of 1.4. The ambient density is then

$$\rho_a = \frac{p_a}{RT_a} = \frac{(15)(144)}{(53.3)(520)(32.2)} = .00242 \text{ slugs}^3/\text{ft}^3$$

The reference sound speed is therefore

$$a_a = \left(\gamma \frac{p}{\rho}\right)^{1/2} = \left\{ \frac{(1.4)(144)(15)}{(.00242)} \right\}^{1/2} = 1115 \text{ ft/sec.}$$

The initial sound speed inside the duct will be taken to have the value:

$$a_o = 1.823\, a_a = 2056.3 \text{ ft/sec}$$

The initial pressure is therefore (equ (22.))

$$p_o = p_a \left(\frac{a_o}{a_a}\right)^{\frac{2\gamma}{\gamma-1}}$$

$$p_o = 15\,(1.823)^7 = 1003.7 \text{ psia}$$
$$= 144{,}531 \text{ psf.}$$

Nondimensional variables will be used in the calculation. In these terms

$$a_a = 1.0 \qquad a_o = 1.823$$
$$p_o = 66.9$$

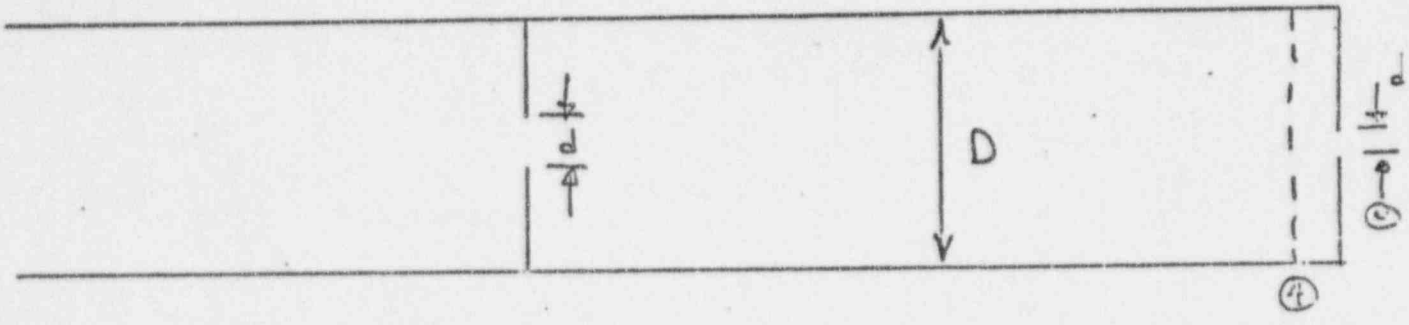

For numerical convenience the ratio of the area of the duct to the area of the opening at the right end is taken to be 57.874. This means D/d' =7.675 and allows D/d =5.0. Since the pressure ratio across the opening is lower than the critical ratio of 0.528 the flow at the exit will be sonic. Therefore, as described earlier,

$$\frac{A_4}{A_c} = \frac{1}{M_4}\left\{\left(\frac{2}{\gamma-1}\right)\left(1+\frac{\gamma-1}{2}M_4^2\right)\right\}^{\frac{\gamma+1}{2(\gamma-1)}}$$

from which we obtain

$$M_4 = 0.01$$

This is the boundary conditon for the right end. As the blowdown of the pipe proceeds this will eventually change but there will be no need to go that far in this example.

The structured wave will be described by a set of five characteristics. The wave diagram is sketched below.

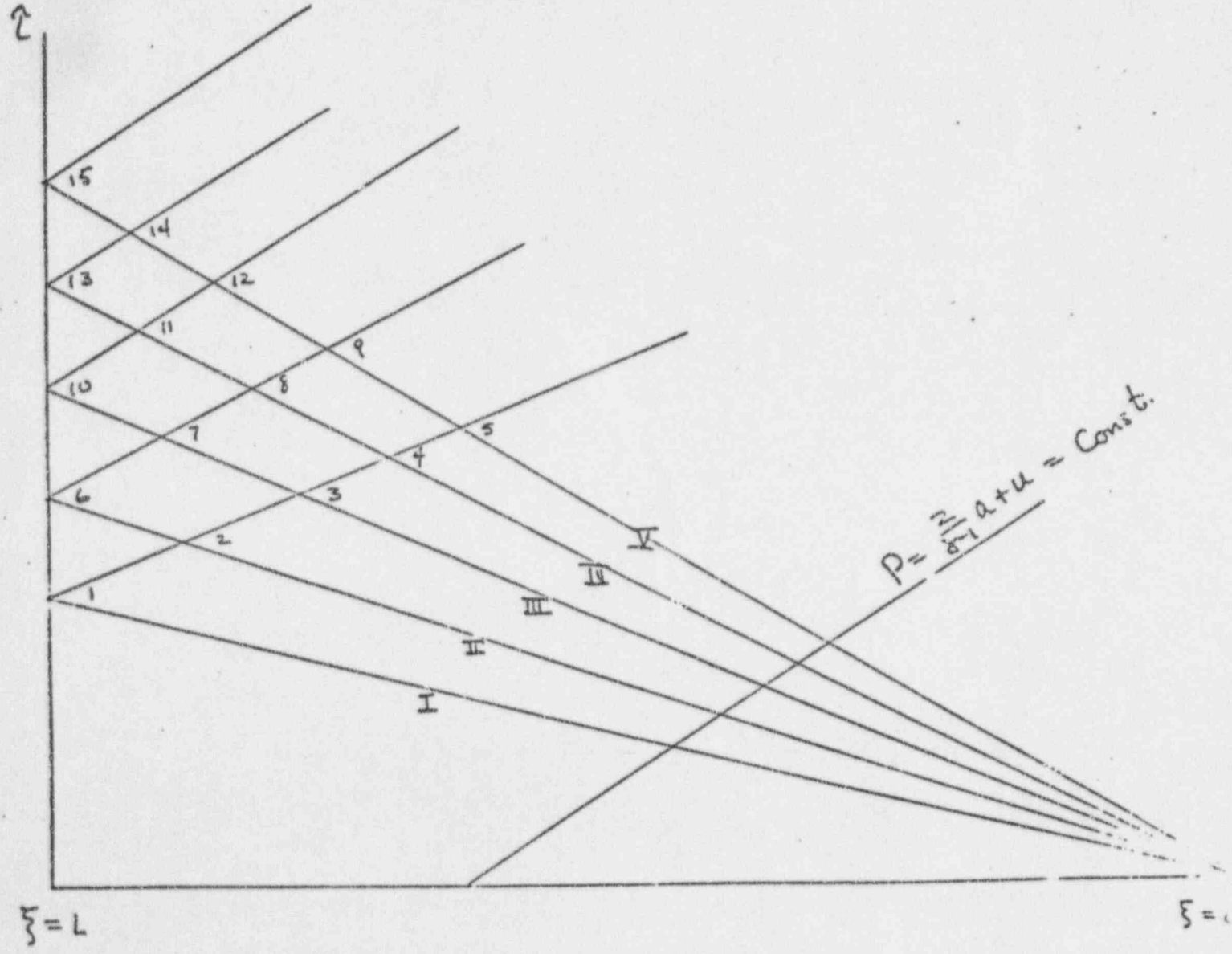

Figure B12

The calculation will be carried out for the 15 points designated on the diagram. The resulting pressure at point 15 is the pressure on the downstream side of the orifice after the first reflection of the wave.

The Q -characteristics that make up the fan are designated I through V. The fluid velocity and sound speed along QV can be calculated from the Mach number at the right boundary and the value of any intersecting P -characteristic which originates on the $\tau = 0$ line. Since in this isentropic region both P and Q are constant it follows that a and u are also constant along each Q characteristic. When the Q -characteristics intercept P -characteristics originating above point 1 however this is no longer true due to the influx of fluid through the orifice.

Thus along QV we have

$$M = \frac{u}{a} = 0.01$$

$$P = \frac{2}{\gamma-1} a + u = \frac{2}{\gamma-1} a_0 = (5)(1.823)$$

$$\therefore \quad 9.115 = 5a + u$$

$$a_{QV} = \frac{9.115}{5.01} = 1.819362$$

$$u_{QV} = .015194$$

We can also now calculate the value of QV

$$QV = 5a_V - u_V = 9.078616$$

The large number of decimal places retained is due to the very small temperature changes occurring in this weak wave.

Since u and a are constant along Q^{I} until after point 5

$$a_5 = 1.819362$$
$$u_5 = 0.018194$$

Calculation of u and a for Q^{I}, and hence point 4, proceeds as follows. Take

$$u_4 = 0.75\, u_5$$
$$= 0.013646$$

The particular value chosen only determines the size of the characteristic net. Again we use the fact that any P-characteristic crossing Q^{IV} between points zero and 4 has the same, known value.

$$P = \frac{2}{\gamma-1} a_0 = 9.115 = \frac{2}{\gamma-1} a_4 + u_4$$

Thus

$$a_4 = 1.820271$$

There again follows

$$Q^{II} = 9.087709$$

Similar calculations determine the values of the variables at the points 3, 2, and 1.

The value of Q and the sound speed at point 2 are now used to calculate the wall point 6 using the iteration procedures outlined earlier. The actual calculation was programmed for a digital computer. The results are shown in the following table. The method that has been described allows the intersection of the characteristics to determine the grid points. These locations can be calculated as follows.

Point	P	Q	u	a	s	b	ξ	τ	u+a	u-a
1	9.115	9.115	0	1.823	0	66.912	1.0	.548546	1.823	-1.82
2	9.115	9.105904	.004548	1.822209	0	66.68	.9985	.549369	1.826638	-1.817
3	9.115	9.096802	.009097	1.821181	0	66.45	996995	.550193	1.830278	-1.812
4	9.115	9.087709	.013646	1.820271	0	66.21	.995484	.551019	1.833917	-1.806
5	9.115	9.078616	.018194	1.819362	0	65.98	.993967	.551846	1.837556	-1.801
6	9.12205	9.109938	.005056	1.822999	.002213	66.71	1.0	.550194	1.828055	-1.817
7	9.11362	9.09966	.009604	1.821282	0	66.47	.9985	.551015	1.830884	-1.8116
8	9.11362	9.087709	.014153	1.820372	0	66.24	.996979	.551846	1.834525	-1.806
9	9.11662	9.078616	.018700	1.819463	0	66.01	.995460	.552674	1.838163	-1.800
10	9.12361	9.106956	.008026	1.822496	.005567	66.39	1.0	.551843	1.831022	-1.814
11	9.11264	9.087709	.01765	1.821072	0	66.42	.998477	.552675	1.838721	-1.803
12	9.11236	9.078616	.017122	1.819148	0	65.93	.996955	.553503	1.836270	-1.802
13	9.12534	9.104605	.010366	1.822994	.009268	66.05	1.0	.553520	1.833360	-1.812
14	9.10244	9.078616	.02336	1.820395	0	66.25	.99848	.554349	1.843755	-1.797
15	9.12732	9.102596	.012362	1.822992	.013154	65.69	1.0	.555195	1.835354	-1.816

Table B1

Results of the Compressible Analysis
(values listed are for nondimensional variables)

Considering the three points shown in the sketch, the coordinates of i can be determined from the coordinates of j and k and the slopes of the characteristics through j and k which intersect at i. The general formula is

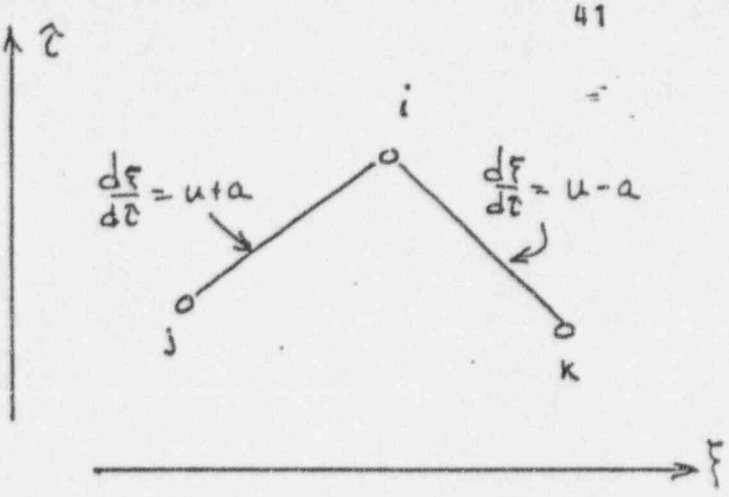

Figure B13

$$\tau_i = \frac{(u+a)_j \tau_j - (u-a)_k \tau_k + \xi_j - \xi_k}{(u+a)_j - (u-a)_k}$$

$$\xi_i = (u+a)_j (\tau_j - \tau_i) + \xi_j$$

Translation of a few pertinent results to dimensional terms will facilitate a comparison with the first analysis. The wave has been completely reflected at point 15. The pressure there is

$$p_{15} = (65.69)(15) = 985.35$$

and

$$u_{15} = (.01236)(1118) = 13.8 \text{ ft/sec.}$$

Thus the difference between p_{15} and the initial pressure is 13.4 psi. Both figures are in excellent agreement with the incompressible results (see pg 12). Since the flow velocity behind the incident wave is only one per cent of the sound speed this is not unexpected.

The difference in time between points 1 and 15 gives an indication of how sharp the pressure rise is. If the orifice is 100 ft. from the open end of the pipe we have

$$t_{15} - t_1 = (.555195 - .548546)\frac{1118}{100}$$

$$t_{15} - t_1 = 0.074 \text{ seconds.}$$

The above analysis does not use the empirical orifice coefficient K. It is, however, implied. It is perhaps of interest to use the results of the analysis to see what value of K would have led to the same thing. We take point 15 as an example

$$p_0 - p_{15} = K \rho_{15} \frac{u_{15}^2}{2}$$

$$K = \frac{2 \Delta p}{\rho u^2}$$

From the equation of state we obtain

$$\rho_{15} = .048 \text{ slugs/ft}^3$$

Thus

$$K = \frac{(2)(18.4)(144)}{(.048)(13.8)^2} = 579.7$$

This agrees very well with the value of 576 used in the incompressible analysis. Again the agreement is to be expected with such low fluid velocities.

The calculation was not continued beyond this point since it was felt that the largest force on the orifice would occur just after the initial reflection. If a longer time history is desired it would be preferable to set up a direct numerical calculation of the entire field. In this case a grid is chosen by selecting a regular array of points in space and a time increment. The intersection of the characteristics from a given point with the previous time line will not be at these pre-selected points and interpolation is necessary. Boundaries are handled as in the above.

C. Empirical Compressible Analysis

In cases where the obstruction is not an orifice it may not be possible to use a non-empirical approach. The following compressible analysis involving the empirical loss factor is therefore also provided. In addition to this generality, the following also turns out to be simpler to apply to what we have referred to as the pipe problem.

Reservoir Problem

The flow through the opening to the atmosphere is handled as before. The treatment of the main flow away from the orifice using characteristics is also the same. In the case of the upstream reservoir the orifice flow can be analyzed as follows.

The empirical relation is

$$p_L - p_{IR} = K \rho_R \frac{u_R^2}{2} \qquad \text{(C1)}$$

where subscripts L and R refer to the upstream (left) and downstream (right) sides of the orifice. The steady flow energy equation is

$$a_L^2 = a_R^2 + \frac{\gamma-1}{2} u_R^2 \qquad \text{(C2)}$$

In addition we have the equation for the Q-characteristic on the right side and the equation of state

$$Q_R = \frac{2}{\gamma-1} a_R - u_R \qquad (C3)$$

$$a_R^2 = \gamma \frac{p_R}{\rho_R} \qquad (C4)$$

These four equations are sufficient to determine u_R, p_R, ρ_R and a_R for a given Q_R. Again an iteration is necessary. Once the state on the right is known the new value of Q_R can be calculated from

$$s_R - s_L = \frac{1}{\gamma-1} \ln \frac{a_R^2}{a_L^2} - \frac{1}{\gamma} \ln \frac{p_R}{p_L} \qquad (C5)$$

$$\delta Q_R = a_R \delta s_R \qquad (C6)$$

The form of the above most useful for the calculation are as follows.

Equation C2 can be written

$$\frac{a_R^2}{a_L^2} = \left\{ 1 + \frac{\gamma-1}{2} M_R^2 \right\}^{-1} \qquad (C7)$$

Equations (C1) and (C4) yield

$$\frac{p_R}{p_L} = \left\{ 1 + \frac{\gamma K}{2} M_R^2 \right\}^{-1} \qquad (C8)$$

Dividing equation (C3) by a_L we obtain

$$\frac{a_R}{a_L} = \frac{Q_R / a_L}{\frac{2}{\gamma-1} - M_R} \qquad \text{(C9)}$$

We now substitute (C9) into (C7) to obtain

$$\left[\left(\frac{\gamma-1}{2}\right)\frac{Q_R^2}{a_L^2} - 1\right] M_R^2 + 2\left(\frac{2}{\gamma-1}\right) M_R + \frac{Q_R^2}{a_L^2} - \left(\frac{2}{\gamma-1}\right)^2 = 0$$

or

$$M_R = \frac{-\frac{2}{\gamma-1} + \sqrt{\left(\frac{2}{\gamma-1}\right)^2 - \left[\frac{\gamma-1}{2}\frac{Q_R^2}{a_L^2} - 1\right]\left[\frac{Q_R^2}{a_L^2} - \left(\frac{2}{\gamma-1}\right)^2\right]}}{\left[\frac{\gamma-1}{2}\frac{Q_R^2}{a_L^2} - 1\right]} \qquad \text{(C10)}$$

The scheme is then to calculate M_R from the assumed value of Q_R in (C10). Then obtain a_R^2/a_L^2 and p_R/p_L (and hence p_R and a_R) from (C9) and (C8). S_R can now be obtained from (C5) (recall that $S_L = 0$), and Q_R calculated from (C6) is checked with the assumed value. If they are not the same it is suggested that the new value of Q_R be obtained from

$$Q_R^{(i+1)} = (1-x)\, Q_R^{(i)} + x\, Q_R^{(c)}$$

where:

$Q_R^{(i+1)}$ = value of Q_R for next iteration

$Q_R^{(i)}$ = value of Q_R from last iteration

$Q_R^{(c)}$ = value of Q_R calculated from $S_R^{(i)}$

x = constant of the order of 0.25

The same numerical example used in the previous two analyses was also used with this approach. Again the iteration was carried out on a digital computer. The most important results for the 4 wall points, (see Figure B12) 6, 10, 13 and 15, are listed below.

POINT	Q	p (psi)	u (ft/sec)
6	9.109919	1000.6	5.65
10	9.106920	995.8	9.01
13	9.104552	990.6	11.65
15	9.102525	985.2	13.9

TABLE C1

(see pg 41)

These results are the same as those of the previous analysis. (Velocities in ft/sec are obtained by multiplying the non-dimensional results in Table B1 by 1118.0. The analogous factor for pressures is 15.0.)

Pipe Problem

The same analysis can be applied to the pipe problem as follows. The pressure drop is again given by

$$p_L - p_R = K \rho_R \frac{u_R^2}{2} \qquad (C11)$$

Conservation of mass and energy through the orifice require

$$\rho_L u_L = \rho_R u_R \tag{C12}$$

and

$$a_L^2 + \frac{\gamma-1}{2} u_L^2 = a_R^2 + \frac{\gamma-1}{2} u_R^2 \tag{C13}$$

In addition we now have two characteristics relations

$$Q_R = \frac{2}{\gamma-1} a_R - u_R \tag{C14}$$

$$P_L = \frac{2}{\gamma-1} a_L + u_L \tag{C15}$$

and two equations of state

$$a_L^2 = \gamma \frac{p_L}{\rho_L} \qquad a_R^2 = \gamma \frac{p_R}{\rho_R} \tag{C16}$$

Finally the flow on the left is isentropic so that $S_L = S_0 = 0$. Therefore by (B22)

$$p_L = (a_L)^{\frac{2\gamma}{\gamma-1}} \tag{C17}$$

The computation scheme proceeds somewhat differently in this case. We first eliminate a_L^p and a_R^p from (C11) using (C16) and (C12)

(C18)

Equations (C14) and (C15) are then used to eliminate a_L and a_R from both (C18) and (C13). The result is the following two coupled quadratics for u_R and u_L .

$$\left\{\frac{\gamma K}{2A_1} + 1 - \frac{u_L}{u_R}\right\} u_R^2 + 2(Q_R + P_L)u_R + Q_R^2 - \frac{u_R}{u_L} P_L^2 = 0, \quad \text{(C19)}$$

where $A_1 = (\gamma - 1/2)^2$,

$$\frac{\gamma-1}{2} u_L^2 - \left(2\,\frac{\gamma-1}{2} P_L\right)u_L + \left\{\frac{\gamma-1}{2}\left(P_L^2 - Q_R^2 - 2Q_R u_R - u_R^2\right) - u_R^2 = 0 \right. \quad \text{(C20)}$$

With assumed values of Q_R (P_L is known) and u_R/u_L we first calculate u_R from (C19). (C20) then yields u_L and the results are compared with the assumed velocity ratio. When this iteration loop is satisfied the remaining variables can be calculated as follows. The upstream sound speed is obtained from (C15). p_L is then obtained from (C17). ρ_L then follows using (C16), and ρ_R from (C12). The downstream pressure is now available from (C11), and a_R from (C13). With all the variables thus determined we again go to (C5) and (C6) to check the assumed value of Q_R and begin that iteration.

Results of this analysis using the same initial wave, etc., as in the previous examples are shown in Table B2. The "points" again refer to Figure B12).

TABLE C2

POINT	P_L (psi)	p_R (psi)	u_L (ft/sec)	u_R (ft/sec)
6	1000.95	999.4	3.97	3.97
10	999.0	994.4	6.53	6.56
13	997.1	979.1	9.18	9.25
15	996.0	983.6	11.21	11.35

Point 15 is seen to agree very well with the results of the incompressible analysis applied to this same case (see pages 10 and 13).

References

1. Contractor, D. N., "The Reflection of Waterhammer Pressure Waves From Minor Losses", Journal of Basic Engineering, Trans ASME, p 445 (June 1965).

2. Jobson, D. A., "On the Flow of a Compressible Fluid through Orifices", Proceedings, Institution of Mechanical Engineers, 169, 37 (1955).

3. Shapiro, A. S., Compressible Fluid Flow, VI, Ronald Press Co., New York (1953).

4. Rudinger, G., Wave Diagrams for Nonsteady Flow in Ducts, D. Van Nostrand Co., Inc., New York (1955).

5. von Mises, R., Mathematical Theory of Compressible Fluid Flow, Academic Press Inc., New York (1958).

6. Anderson, G. D., and Band, W., "Compressible Fluid Flow and the Theory of Characteristics", American Journal of Physics, p 831-837 (1964).

7. Courant, R., and Friedrichs, K. O., Supersonic Flow and Shock Waves, Interscience Publishers Inc., New York (1948).

8. Keenan, J. H., and Kaye, J., Gas Tables, John Wiley & Sons Inc., New York (1945).

9. Hall, W. B., and Orme, E. M., "Flow of a Compressible Fluid Through a Sudden Enlargement in a Pipe", Proceedings, Institution of Mechanical Engineers, 169, 1007 (1955).

10. Shames, I. H., Mechanics of Fluids, McGraw-Hill Book Company, Inc., New York (1962).

ASME TRANSACTIONS. JOURNAL of BASIC ENGINEERING
(JUNE 1965) pp. 445-452.

Chapin

The Reflection of Waterhammer Pressure Waves From Minor Losses

D. N. CONTRACTOR
Research Scientist,
Hydronautics, Inc.,
Laurel, Md.

This paper deals with the reflection produced when a waterhammer pressure wave encounters any device that produces a sudden energy loss such as an orifice, a valve, or an elbow. The classical wave theory is used to determine the magnitudes of the reflected and the transmitted waves.

The waterhammer equations, with the friction term included, are solved by the method of characteristics. The conditions at a minor loss are studied as a boundary condition to these equations.

Agreement between theoretical and experimental pressure-time diagrams is sufficient to validate the theory.

Introduction

WATERHAMMER in a pipe system can be analyzed in many ways. There is the numerical method in which the head and velocity at a particular section in the pipeline are obtained by a careful bookkeeping of the passage of waterhammer waves and their reflections past that section. In this elementary form of waterhammer analysis, it is imperative to know the magnitude of the reflection of waterhammer waves at certain boundary conditions, such as changes in pipe diameter, pipe-wall thickness, and pipe-wall material. The reflections at certain end conditions must also be known, such as at a constant head reservoir or at a dead end. These reflections have been known and used for a long time [1, 2].[1] In this paper, we examine the reflection and transmission that occur when a waterhammer wave encounters a device that produces a sudden energy loss during steady flow, such as at an orifice, a pipe bend, or a partly closed valve.

The second method of waterhammer analysis is graphical in nature. In this method, the slopes of two characteristic lines are determined, and, knowing the initial and boundary conditions of the pipeline, the head and velocity can be determined as a function of time. This method automatically takes account of the reflection and transmission of waterhammer waves at any boundary or end conditions. Thus this paper does not present anything that is useful to this method. In fact, the conditions at a minor loss can be taken into account by this method of solution. However, despite the fact that the final solution is obtained, the graphical method does not give one a clear insight into the mechanics of the problem.

The most recent and versatile method of obtaining solutions of the waterhammer equations makes use of the method of characteristics. This procedure is able to take into account a continuous distribution of fluid friction in the pipe and provide the pressure and velocity at regular intervals along the pipe as a function of time. A program for a high-speed computer can be written with ease using the characteristic equations and appropriate boundary conditions. In working out the equations at a minor loss as a boundary condition, it will be seen that the conclusions reached earlier are verified.

Elementary Solution

The theoretical study of waterhammer reduces to the solution of two partial differential equations. These equations have been derived by many writers [1, 2, 3] and will be used directly in this paper. The first equation is derived from the condition of dynamic equilibrium:

$$\frac{\partial H'}{\partial x'} = -\frac{1}{g}\frac{\partial V'}{\partial t'} \tag{1}$$

where the notation used is presented at the beginning of the paper.

The second equation is derived from considerations of continuity in a horizontal pipe:

$$\frac{\partial H'}{\partial t'} = \frac{-a^2}{g}\frac{\partial V'}{\partial x'} \tag{2}$$

where a represents the wave celerity in the pipe.

The simultaneous solution of these two equations is given by

$$H' - HO = F\left(t' + \frac{x'}{a}\right) + f\left(t' - \frac{x'}{a}\right) \tag{3}$$

and

$$V' - VO = -\frac{g}{a}\left\{F\left(t' + \frac{x'}{a}\right) - f\left(t' - \frac{x'}{a}\right)\right\} \tag{4}$$

In the foregoing equations, F and f are arbitrary functions and can be evaluated at points where V' and H' are known and then used to find V' and H' at other points in the same pipe. These

[1] Numbers in brackets designate References at end of paper.

Contributed by the Fluids Engineering Division and presented at the Winter Annual Meeting, New York, N. Y., November 29–December 3, 1964, of THE AMERICAN SOCIETY OF MECHANICAL ENGINEERS. Manuscript received at ASME Headquarters, August 8, 1964. Paper No. 64—WA/FE-16.

Nomenclature

a = wave celerity in pipe
A = cross-sectional area of pipe
A_g = area of gate valve
C_d = coefficient of discharge
D = diameter of pipe
f = Darcy-Weisbach friction factor
f, f_r, f_s = waterhammer, pressure wave heights
g = gravitational acceleration
H = piezometric head
H = dimensionless piezometric head = H'/HO
HO = head causing flow
K = loss coefficient of orifice
L = length of pipeline
MLOSS = minor loss
t' = time
t = dimensionless time = $t'/2L/a$
V' = velocity of water in pipe
V = dimensionless velocity = V'/VO
VO = steady-state velocity
x' = distance from reservoir
x = dimensionless distance = x'/L
β = waterhammer constant = $aVO/2gHO$
Δ = difference or change
τ = ratio of effective gate opening to full gate opening = $\frac{(C_dA_g)_{t=t}}{(C_dA_g)_{t=0}}$

equations are used to find the reflection and transmission of a pressure wave when it encounters a minor loss.

In Fig. 1, let points A and B be on either side of the loss-producing device, for example an orifice. Let F_1 be a waterhammer pressure wave approaching point A. Let f_1 be its reflection and F_2 its transmission. Let the head and velocity before F_1 reaches the orifice be H'_{A0}, H'_{B0} and V'_{A0}, V'_{B0}; and let the head and velocity after reflection and transmission be H'_{A1}, H'_{B1} and V'_{A1}, V'_{B1}.

From equations (3) and (4)

$$H'_{A1} - H'_{A0} = F_1 + f_1 \tag{5}$$

$$H'_{B1} - H'_{B0} = F_2 \tag{6}$$

$$V'_{A1} - V'_{A0} = -\frac{g}{a}(F_1 - f_1) \tag{7}$$

$$V'_{B1} - V'_{B0} = -\frac{g}{a} F_2 \tag{8}$$

If the pipe diameter is the same before and after the orifice, then continuity requires

$$V'_{A1} = V'_{B1} \quad \text{and} \quad V'_{A0} = V'_{B0} \tag{9}$$

Since a minor loss occurs at the orifice

$$H'_{B0} - H'_{A0} = \text{MLOSS}_0 \quad \text{and} \quad H'_{B1} - H'_{A1} = \text{MLOSS}_1$$

From the above equations, it can be shown that

$$f_1 = \frac{1}{2}(\text{MLOSS}_0 - \text{MLOSS}_1) = \frac{-\Delta(\text{MLOSS})}{2} \tag{10}$$

and

$$F_2 = F_1 + \frac{\Delta(\text{MLOSS})}{2} \tag{11}$$

Thus it is seen that the reflection is dependent only upon the change in the minor loss before and after the passage of the wave. The transmitted wave is equal to the approaching wave plus half the change in the minor loss.

The change in the minor loss is easily evaluated when the velocity behind the approaching wave F_1 is zero or very nearly zero. This is so when instantaneous closure of the valve occurs and the pipeline is considered frictionless. For this case

$$\Delta(\text{MLOSS}) = -KV_{A0}^2/2g \tag{12}$$

Hence

$$f_1 = \tfrac{1}{2}KV_{A0}^2/2g \tag{13}$$

nd

$$F_2 = F_1 - \tfrac{1}{2}KV_{A0}^2/2g \tag{14}$$

However, when the velocity behind the wave F_1 is not zero, equations (13) and (14) do not apply and f_1 becomes a more complicated function of F_1. This relationship is found in the following manner:

Let

$$\text{MLOSS}_0 = K\frac{V_{A0}^2}{2g} = K\frac{V_{B0}^2}{2g}$$

and

$$\text{MLOSS}_1 = K\frac{V_{A1}^2}{2g} = K\frac{V_{B1}^2}{2g}$$

Therefore

$$\Delta(\text{MLOSS}) = \frac{K}{2g}\{V_{A1}^2 - V_{A0}^2\}$$

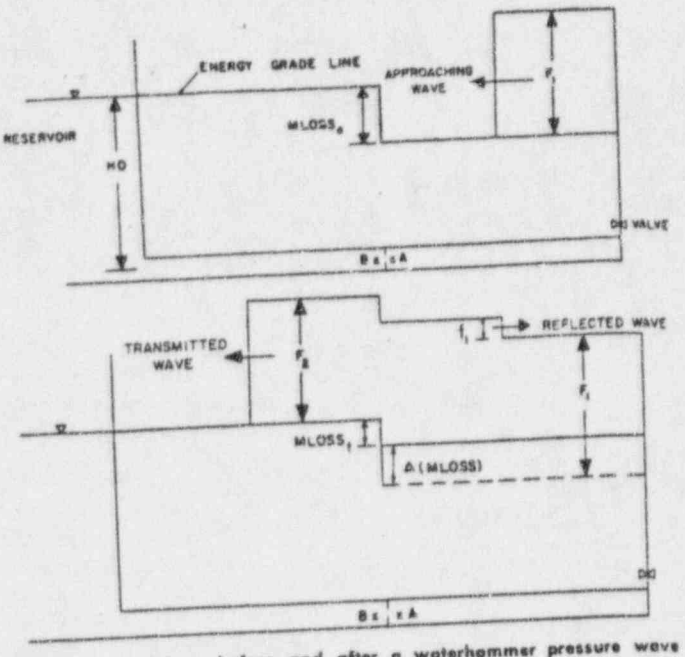

Fig. 1 Conditions before and after a waterhammer pressure wave encounters a minor loss

Using the foregoing relationships and solving for f_1 and F_2

$$f_1 = F_1 - \frac{a}{g}\left\{\frac{2a}{K} + V_{A0}\right\} + \frac{a}{g}\sqrt{\left(\frac{2a}{K} + V_{A0}\right)^2 - \frac{4gF_1}{K}} \tag{15}$$

and

$$F_2 = \frac{a}{g}\left(\frac{2a}{K} + V_{A0}\right) - \frac{a}{g}\sqrt{\left(\frac{2a}{K} + V_{A0}\right)^2 - \frac{4gF_1}{K}} \tag{16}$$

The procedure is the same when analyzing the situation in which an f_1 wave approaches a minor loss, as in the case of flow establishment in a pipe. It can be shown that the reflected wave $F_1 = \dfrac{-\Delta(\text{MLOSS})}{2}$ and that the transmitted wave $f_2 = f_1 + \dfrac{\Delta(\text{MLOSS})}{2}$.

More complicated situations can also be handled in the same manner. For example, consider the situation in which an F_1 wave approaches a minor loss from the right-hand side and an f_2 wave approaches it from the left-hand side and both the waves encounter the minor loss at the same time. It can be shown that the reflected wave on the right-hand side $f_1 = f_2 - \Delta(\text{MLOSS})/2$ and that the reflected wave on the left-hand side $F_2 = F_1 + \Delta(\text{MLOSS})/2$.

Solution of Waterhammer Equations by the Method of Characteristics

The partial differential equations for waterhammer in a pipe, taking into account fluid-friction effects, have been derived elsewhere [4, 5] and will be used directly here. These equations are quasi-linear, hyperbolic partial differential equations, and since they have two real characteristics, the method of characteristics can be used for their solution. These equations are given as follows:

The condition of dynamic equilibrium:

$$\frac{\partial H'}{\partial x'} + \frac{f}{D}\frac{(V')^2}{2g} = -\frac{1}{g}\left\{\frac{\partial V'}{\partial t'} + V'\frac{\partial V'}{\partial x'}\right\} \tag{17}$$

The condition of continuity for horizontal pipes:

$$\frac{\partial H'}{\partial t'} + V'\frac{\partial H'}{\partial x'} = -\frac{a^2}{g}\frac{\partial V'}{\partial x'} \tag{18}$$

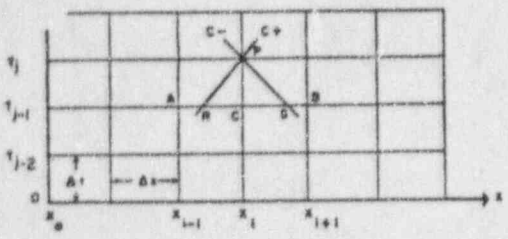

Fig. 2 The (x, t) plane for a uniform pipe

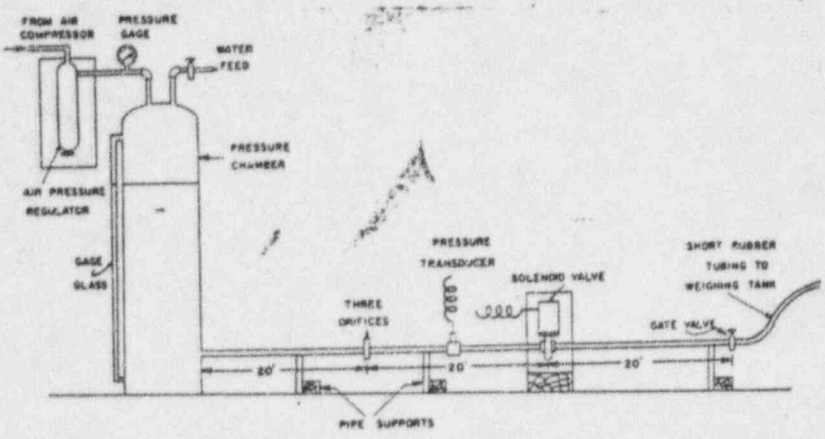

Fig. 3 Schematic diagram of experimental setup

These equations are made dimensionless by the use of certain constants. The dimensionless parameters are given as

$$H = \frac{H'}{HO'}, \quad V = \frac{V'}{VO'}, \quad x = \frac{x'}{L}, \quad \text{and} \quad t = \frac{t'}{2L/a}$$

As shown by previous writers [4, 5], the partial differential equations (17) and (18) can be replaced by four total differential equations that describe two characteristics. By making the assumption that $VO \ll a$ and writing $\beta = a\,VO/2gHO$, these equations can be written in finite-difference form by integrating from point 0 to point 1 along each characteristic.

Thus, along the C_+ characteristic

$$(x_1 - x_0) - 2(t_1 - t_0) = 0 \tag{19}$$

and

$$(V_1 - V_0) + (H_1 - H_0)/2\beta + \frac{LVO}{aD}(fV^2)_0(t_1 - t_0) = 0 \tag{20}$$

along the C_- characteristic

$$(x_1 - x_0) + 2(t_1 - t_0) = 0 \tag{21}$$

and

$$(V_1 - V_0) - (H_1 - H_0)/2\beta + \frac{LVO}{aD}(fV^2)_0(t_1 - t_0) = 0 \tag{22}$$

If the friction term is neglected in equations (20) and (22), it can be seen that these are the equations used in the graphical analysis of waterhammer.

The equations for the pressure and velocity at a point in a uniform pipe have been derived from equations (19) to (22) by previous authors [4, 5]. Let P be the point at which the pressure and velocity are to be determined. (See Fig. 2). Then it can be shown that

$$H_P = (H_A + H_B)/2 - (V_B - V_A)\beta + \beta\frac{LVO\Delta t}{aD}\{(fV^2)_B - (fV^2)_A\} \tag{23}$$

$$V_P = (V_A + V_B)/2 - (H_B - H_A)/4\beta - \frac{LVO\Delta t}{2aD}\{(fV^2)_A + (fV^2)_B\} \tag{24}$$

Similar equations can be derived for the end points of a pipeline by combining the appropriate characteristic with the particular end conditions. These equations will not be presented here as they are not of immediate interest. However, conditions at the location of a minor loss in a uniform pipeline will be studied in detail.

Boundary Conditions at a Minor Loss

Consider two points P_1 and P_2 just upstream and downstream of a minor loss. The velocity and pressure at these two points can be determined by solving four equations. Two of them are the characteristic equations (20) and (22). The other two are the continuity and energy equations between P_1 and P_2. The final solutions are given as follows:

$$H_{P_1} = (H_A + H_B)/2 - \beta(V_B - V_A) + \beta\frac{LVO\Delta t}{aD}\{(fV^2)_B - (fV^2)_A\} + \frac{1}{2}\frac{KVO^2}{2gHO}V_{P_1}^2 \tag{25}$$

$$H_{P_2} = (H_A + H_B)/2 - \beta(V_B - V_A) + \beta\frac{LVO\Delta t}{aD}\{(fV^2)_B - (fV^2)_A\} - \frac{1}{2}\frac{KVO^2}{2gHO}V_{P_1}^2 \tag{26}$$

$$V_{P_1} = V_{P_2} = (V_A + V_B)/2 + (H_A - H_B)/4\beta - \frac{LVO\Delta t}{2aD}\{(fV^2)_A + (fV^2)_B\} - \frac{1}{2\beta}\frac{1}{2}\frac{KVO^2}{2gHO}V_{P_1}^2 \tag{27}$$

It can be seen that the first three terms of equations (25) and (26) are identical with equation (23) for a uniform pipeline. The last term is equal to half the dimensionless minor loss and accounts for the reflection that takes place. The magnitude of the reflection is seen to be the same as indicated in equation (13).

Experimental Verification

An experiment was devised to check the validity of the equations derived for conditions at a minor loss. The experiment was organized in such a way that the reflected wave could be recorded and compared with the minor loss. In order to make the reflection large, the minor loss also had to be made as large as possible and, hence, a device was chosen with a very large loss coefficient. This device was placed in the middle of a pipeline and the pressure at different points was recorded and compared with the theoretical pressure-time history.

A schematic of the experimental setup is shown in Fig. 3. At one end of the pipeline is a compression chamber, half filled with water and with compressed air above it. The pressure of the air is always maintained at a constant level by means of a pressure regulator placed between the chamber and the compressor. Twenty ft from the pressure chamber, three closely spaced orifices are placed in the pipeline to produce a large loss. Steady-state experiments conducted on the orifices determined the loss coefficient to be 1150 over a Reynolds number range of 600–10,000. This steady-state loss coefficient was used in the computer program for the calculation of the theoretical pressures and velocities.

A quick-acting solenoid valve, placed twenty ft from the orifices, was used to produce the waterhammer waves. For use in the theoretical calculation of pressures and velocities in the pipe, it was necessary to determine such characteristics of the valve as rate and time of closure and the variation of the hydraulic resistance of the valve as it closed. The hydraulic resistance of the valve was determined statically by measuring the pressure drop across the valve as the sliding gate of the solenoid

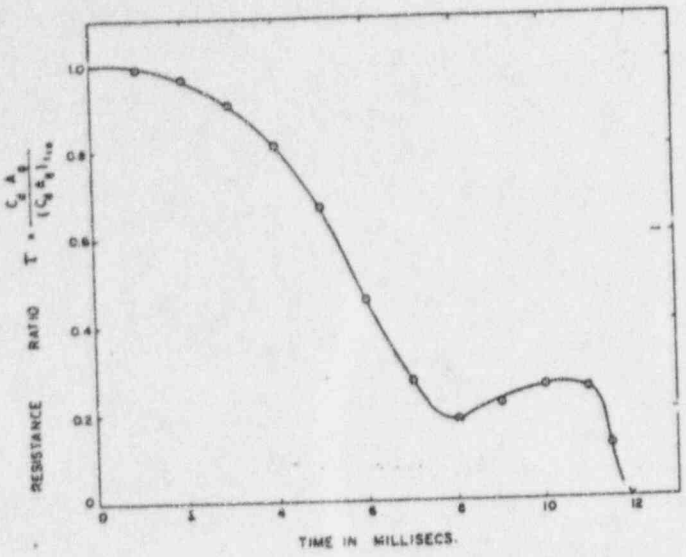

Fig. 4 Resistance of solenoid valve during closure

valve was depressed in small steps. The rate and time of closure were determined electronically. The hydraulic resistance of the valve as a function of time is given in Fig. 4. It can be seen that the valve closed in 12.0 millisec. The return-travel time of the wave, $2L/a$, for this pipeline is 18.0 millisec.; hence, this was a case of rapid closure of the valve.

Twenty ft downstream from the solenoid valve, the pipeline was terminated by a gate valve. This valve was operated in such a way as to elevate the static pressure in the pipeline and keep the velocity of the water low. This additional pipeline was felt necessary to prevent any reflections from downstream traveling past the solenoid valve while it was closing. In this way, the pressure wave in the main pipeline was kept free of any extraneous disturbances.

The pressure transducer used was of the strain gage type and was mounted so as to make the sensitive face tangential to the inside of the pipe. The transducer was connected to an Ellis bridge amplifier, which also provided the input for the Wheatstone bridge in the transducer. The output of the amplifier was fed into an oscilloscope, and a polaroid camera mounted on the oscilloscope recorded the wave pattern.

Three pressures were recorded during each experiment: first, the head HO causing flow in the pipeline; second, the static pressure at that point under steady-flow conditions; and last, the waterhammer pressure in the pipe due to sudden closing of the solenoid valve. The difference in the two static pressures is the loss that occurs at the orifices. This can be compared to the wave reflected from the orifices. Typical recordings of such experiments are given in Figs. 5 and 6.

The following experiments were conducted:

1 Pipeline with a minor loss in the middle

(a) Turbulent flow: pressure transducer at $x' = 3L/4 = 30'$.
(b) Turbulent flow: pressure transducer at $x' = L = 40'$.
(c) Laminar flow: pressure transducer at $x' = 3L/4 = 30'$.

2 Straight pipeline

(a) Turbulent flow: pressure transducer at $x' = 3L/4 = 30'$.

Computer Program

Using the equations derived from the method of characteristics and the experimentally determined characteristics of the solenoid valve, the theoretical pressure and velocity at regular intervals along the pipe were calculated as a function of time. A high-speed electronic computer (IBM 7090) was used for the arithmetical integration of the waterhammer equations. The results from the computer program were plotted with the experimental results for comparison.

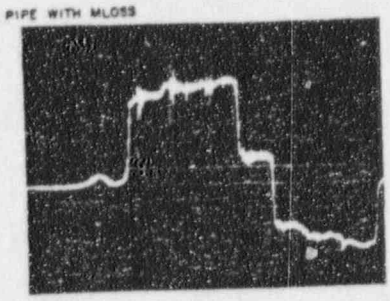

FIGURE 5. WATER-HAMMER PRESSURE-TIME RECORDING AT x = 3L/4

CASE 1(a), 1 CYCLE
TEMP. = 78° F
HO = 194 FT
VO = 1.20 FPS
PRESSURE SCALE 1 cm = 30 PSI
TIME SCALE 1 cm = 5 m SECS

Fig. 5 Waterhammer pressure-time recording: case 1(a): one cycle

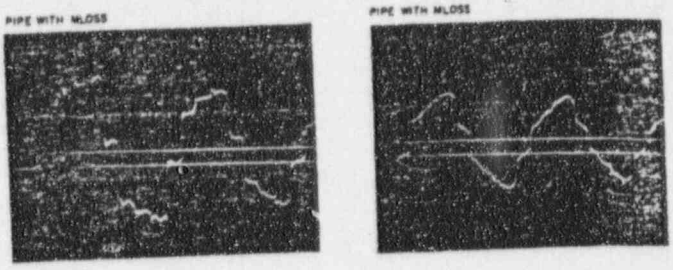

FIGURE 6. WATER-HAMMER PRESSURE-TIME RECORDING AT x = 3L/4

CASE 1(a), 4 CYCLES
TEMP. = 78° F
HO = 194.0 FT
VO = 1.2 FPS
PRESSURE SCALE 1 cm = 5 PSI
TIME SCALE 1 cm = 10 m SECS

Fig. 6 Waterhammer pressure-time recording: case 1(a): four cycles

Discussion of Results

The experimental and theoretical pressure wave forms are superimposed in Figs. 7 to 12 for comparison. For all cases, four cycles of the pressure wave have been reproduced. In addition to this, pressure-time diagrams of one cycle have also been presented for the case of the pipeline with a minor loss in the middle. In this way, it is possible to see the magnitude of the reflection in the one-cycle diagram and compare it with the minor loss and also observe its influence on the decay of the pressure wave in the four-cycle diagram.

It was the intention of the author to obtain a wave form with as few disturbances as possible so that the reflection of the wave could be noticed easily. It was for this reason that a pump was not used at the upstream end and a compression chamber with compressed air was thought necessary. However, there were some disturbances that could not be eliminated. The way in which the solenoid valve closed produced one such disturbance that appears in every cycle of the wave and was taken into account in the theoretical program.

It can be seen that, in every case, the experiment and theory agree in the first half of the first cycle. There is agreement both in magnitude and form of the wave. In Figs. 7 and 9 the reflection from the minor loss can be seen and compared with the steady-state minor loss. It is only in this part of the diagram that the theoretical program exactly depicts the experimental conditions.

When the pressure in the pipeline falls below the static head HO for the first time, air that was dissolved in the water at the static head HO is liberated and begins to cushion the wave front. This effect can be seen in all of the remaining cycles by the discrepancy which develops between the experimental and theoretical traces. This situation is more pronounced in the case of the pipeline with a minor loss than in the straight pipeline

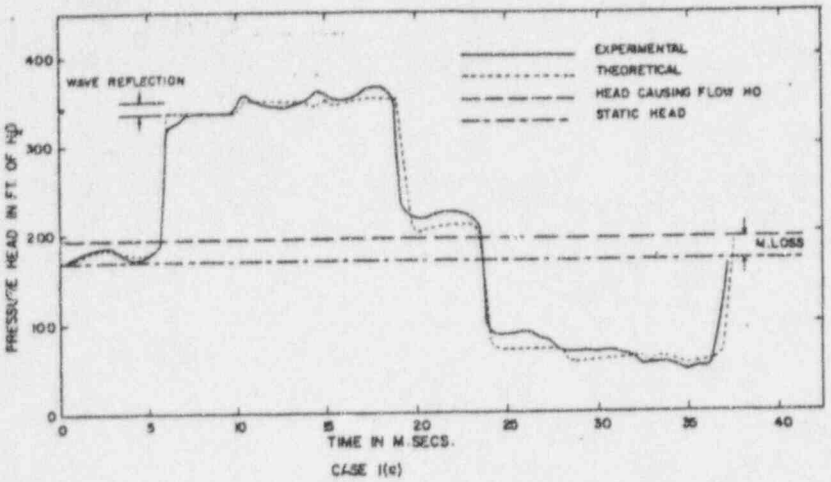

Fig. 7 Waterhammer pressure-time diagram; case 1(a): one cycle

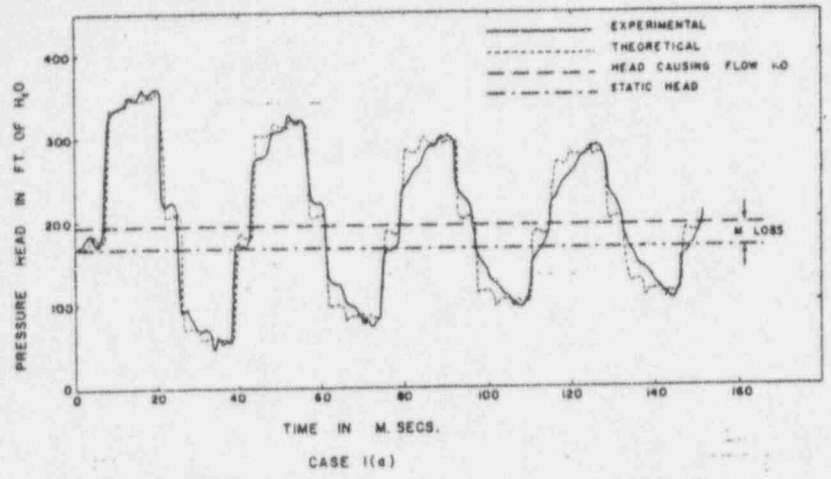

Fig. 8 Waterhammer pressure-time diagram; case 1(a): four cycles

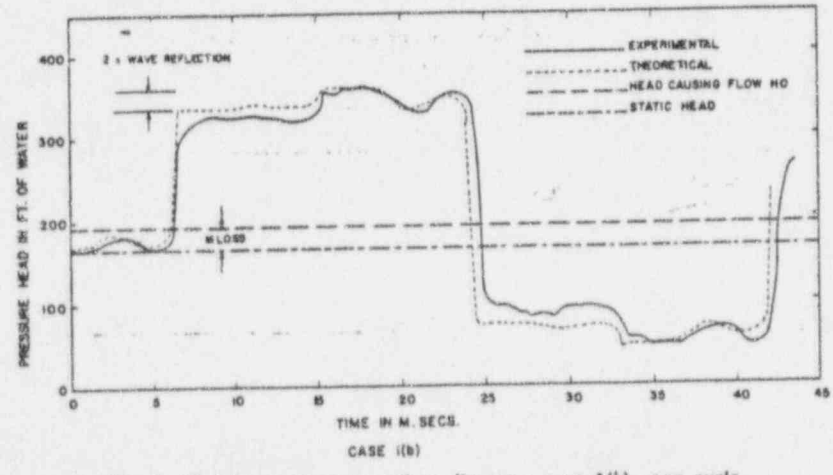

Fig. 9 Waterhammer pressure-time diagram; case 1(b): one cycle

This is so because the constriction at the orifices produces a far lower pressure than in the case of the straight pipeline and, consequently, more dissolved air is set free.

There are several reasons to make one believe that the difference between the theoretical and experimental curves was due to gas liberation alone. First, the water used in the experiment was drawn from the sump in the laboratory. This water is far from pure, as many additives are added for various purposes, such as rust-preventives and algae inhibitors. These compounds, like chlorox and dilute hydrochloric acid, when dissolved in water introduce gases like chlorine, making the water more susceptible to gas liberation when subject to low pressures. Second, at the end of each experiment, bleeding of the pipeline at the orifice and at the valve would indicate the presence of small bubbles. Third, the discrepancy occurs only after the first drop in pressure below static pressure. The discrepancy cannot be attributed to an incorrect value of the steady-state loss coefficient or to the fact that the unsteady loss coefficient was not used, since the same type of discrepancy exists in the case of the straight pipeline. Finally, the nature of the discrepancy itself leads one to recognize it as one of gas liberation. In nearly all the cases, gas bubbles act as a spring that cushions the pressure change, allowing the maximum pressure to be reached only after some time.

For the case of laminar flow, it can be seen that the calculated and actual wave speeds do not differ by more than 1 percent. This is in contrast to the experimental results reported in reference

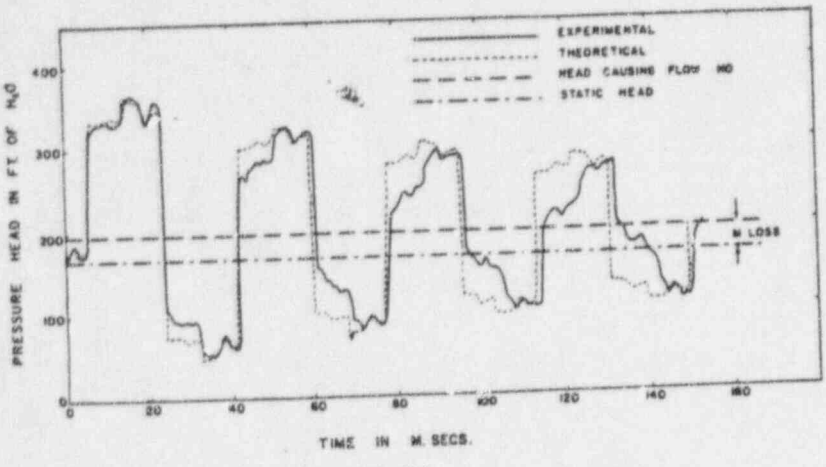

Fig. 10 Waterhammer pressure-time diagram; case 1(b): four cycles

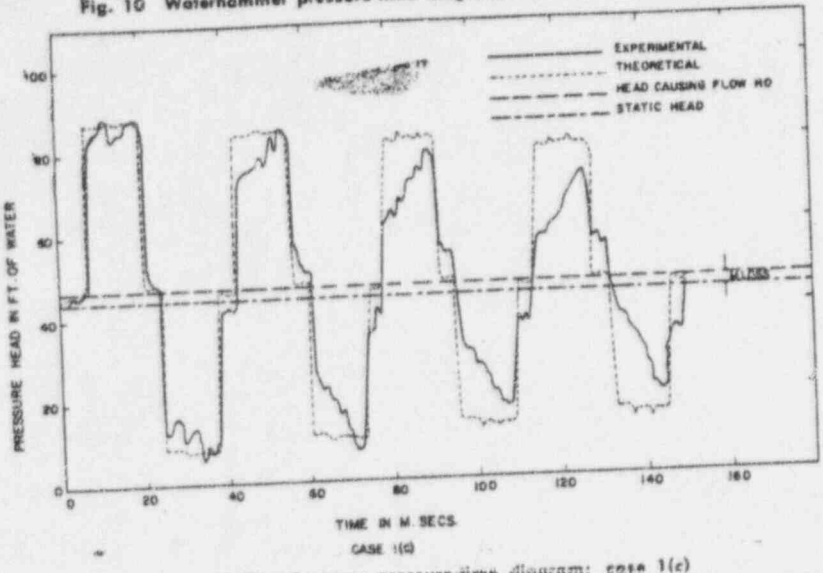

Fig. 11 Waterhammer pressure-time diagram; case 1(c)

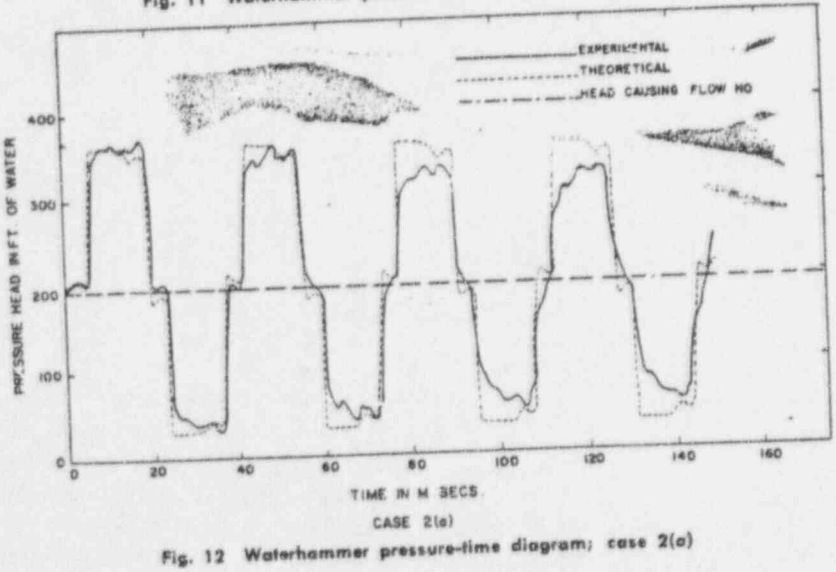

Fig. 12 Waterhammer pressure-time diagram; case 2(a)

[5]. The magnitude of the pressure wave also agrees fairly well with theoretical results, despite the assumption of uniform velocity distribution over the pipe area. However, it is not possible to see the reflection from the minor loss because of the small magnitude of the loss. A more elaborate theoretical study of waterhammer in laminar flow is presented by Rouleau [6]. However, in the experimental verification of his theory, he used oil flowing in a pipeline, and because of the volatile constituents of the oil, the experimental and theoretical traces did not match well.

Conclusions

Whenever a waterhammer wave encounters a device causing a sharp energy loss, a reflection is sent back from it. The magnitude of this reflection is equal to $-\Delta(\text{MLOSS})/2$. The wave transmitted on is equal to the value of the approaching wave plus $\Delta(\text{MLOSS})/2$.

The method of characteristics is a very simple and efficient way to provide particular solutions for the waterhammer equations including friction effects. When setting up a computer program

for waterhammer in a pipeline with a minor loss in it, conditions at the minor loss must be treated as a boundary condition. The equations at the boundary condition verify the conclusions about the magnitude of the reflected wave, reached earlier. It is sufficiently accurate to use the steady-state loss coefficients of the ..., at least for the case of instantaneous and rapid gate ...es, even though waterhammer is a markedly unsteady phenomenon.

Acknowledgments

This work was carried out under the sponsorship of the National Science Foundation Grant GP-340 at the University of Michigan.

The author wishes to express his gratitude to Prof. V. L. Streeter for suggesting this problem, for his support and encouragement. The author thanks the University of Michigan Computing Center for the use of the IBM 7090 computer.

References

1 J. Parmakian, *Water-Hammer Analysis*, Prentice-Hall Inc., New York, N. Y., 1955.

2 G. R. Rich, *Hydraulic Transients*, McGraw-Hill Book Company, Inc., New York, N. Y., first edition, 1951.

3 Symposium on Water-Hammer, ASME-ASCE, 1933

4 V. L. Streeter, "Valve Stroking to Control Water Hammer," *Journal of the Hydraulics Division*, Proc. of the ASCE, vol. 89, no. HY2, March, 1963.

5 V. L. Streeter and Lai Chintu, "Water-Hammer Analysis Including Fluid Friction," ASCE Proc., Paper 3135, May, 1962.

6 W. T. Rouleau, "Pressure Surges in Pipelines Carrying Viscous Liquids," JOURNAL OF BASIC ENGINEERING, TRANS. ASME, Series D, vol. 83, 1960, pp. 912–920.

DISCUSSION

C. B. Wylie[2]

The author has made a significant contribution to the literature with this presentation of theory and experiment on the topic of minor losses in pipe lines subjected to waterhammer. The writer would like to elaborate on the conclusions of the paper by presenting the equations for the computer solution in a different and more convenient form. Supplemental information concerning the inclusion of the velocity head in the computations also is included herein.

In the solution of a practical problem, the conditions at a minor loss are treated as a boundary condition. As pointed out by the author, equations (23) and (24) can be combined, yielding a form suitable for use at boundary conditions. They can be written in the following dimensionless form:

$$V_{P_1} = C_3 - \frac{1}{2\beta_1} H_{P_1} \tag{28}$$

$$V_{P_2} = C_4 + \frac{1}{2\beta_2} H_{P_2} \tag{29}$$

where

$$C_3 = V_R + \frac{H_R}{2\beta_1} - \frac{L_1 V O_1 \Delta t}{a_1 D_1} (fV^2)_R \tag{30}$$

and

$$C_4 = V_S - \frac{H_S}{2\beta_2} - \frac{L_2 V O_2 \Delta t}{a_2 D_2} (fV^2)_S \tag{31}$$

The notation is the same as that of the authors, with the subscripts 1 and 2 referring to the locations upstream and downstream of a ...or loss or boundary condition. The magnitude of C_3 and C_4 ...ust be evaluated during each computational period from system constants and current values of the variables. Continuity conditions at the minor loss yields

$$V_{P_1} A_2 = V_{P_2} A_1 \tag{32}$$

and the minor loss equation gives

$$H_{P_1} - H_{P_2} + K \frac{VO^2}{2gHO} V_{P_1}^2 \tag{33}$$

or

$$H_{P_1} = H_{P_2} + K C_5 V_{P_1}^2 \tag{34}$$

The set of simultaneous equations (28), (29), (32), and (34), can be solved explicitly for one of the velocities and then for each of the other three unknowns. The solution of the quadratic equation resulting from a combination of these equations is

$$V_{P_1} = \frac{1}{KC_5}\left[-\left(\beta_1 + \frac{A_1}{A_2}\beta_2\right) + \sqrt{\left(\beta_1 + \frac{A_1}{A_2}\beta_2\right)^2 + 2KC_5(C_3\beta_1 + C_4\beta_2)} \right] \tag{35}$$

The form of equations (28) and (29) is identical to that used at any boundary condition. Therefore, this set of equations is somewhat more desirable than equations (25), (26), and (27), which are written for a minor loss in a constant diameter pipe. Identical results would be obtained using either set of equations for a case of minor loss in a pipe of uniform characteristics.

One of the assumptions in the development of the general waterhammer equations (1) and (2) is that the velocity head is negligible when compared with the pressure changes. Thus, the total head used in the equations refers to the hydraulic grade line rather than the energy grade line. Using the characteristics solution on the computer, it is not necessary to make this assumption. In most practical situations, the assumption leads to no appreciable error; however, if a case is being treated in which minor losses are significant, it also may be true that the velocity head should be considered.

Two examples follow to illustrate the treatment of boundary conditions with the velocity head taken into consideration. The first example is an entrance condition with little or no minor loss; the second is an abrupt expansion with the appropriate minor loss included.

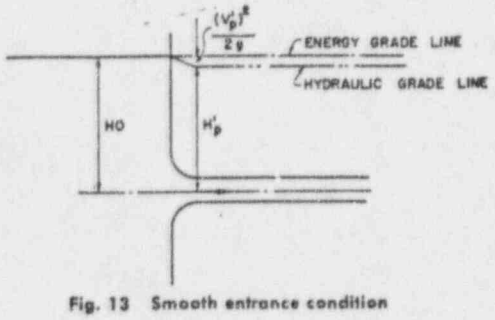

Fig. 13 Smooth entrance condition

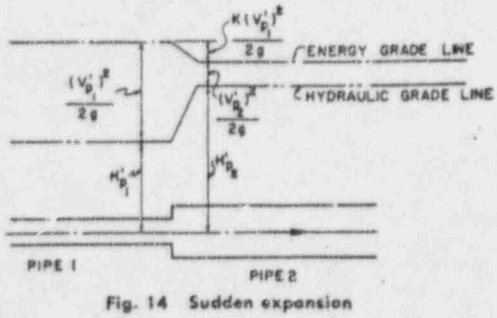

Fig. 14 Sudden expansion

[2] Research Associate, Civil Engineering Dept., University of Michigan, Ann Arbor, Mich.

The boundary condition shown in Fig. 13, illustrating a smooth entrance condition, can be described by equation (29) and an expression of the energy relationship at the entrance:

$$HO = H_P' + \frac{(V_P')^2}{2g} \tag{36}$$

In dimensionless form, this equation becomes

$$H_P = 1 - C_4 V_P^2 \tag{37}$$

The abrupt expansion shown in Fig. 14 can be described by equations (28), (29), (32), and the Bernoulli equation, including the minor loss,

$$H_{P_1}' + \frac{(V_{P_1}')^2}{2g} = H_{P_2}' + \frac{(V_{P_2}')^2}{2g} + \frac{K(V_{P_1}')^2}{2g} \tag{38}$$

In dimensionless form, the last equation becomes

$$H_{P_1} + C_4 V_{P_1}^2 = H_{P_2} + C_4 V_{P_2}^2 + K C_4 V_{P_1}^2 \tag{39}$$

These four equations can be solved easily for the four unknowns at the junction. The provision to handle a flow reversal also can be included without difficulty.

A similar approach can be used to obtain a solution including the velocity head at any boundary condition or minor loss.

Author's Closure

The author wishes to thank Mr. E. B. Wylie for his discussion. The velocity head term could easily be handled in the equations as shown by him in equations (37) and (39). Like the minor loss terms the velocity-head terms are taken into account without approximation or linearization, and this fact is one of the advantages of the method of characteristics.

IME. PROC., 169:37(1955) 767-776.

On the Flow of a Compressible Fluid through Orifices

By D. A. Jobson*

By making certain basic assumptions, the author has determined a theoretical expression for the contraction coefficient, C, appropriate to an orifice when transmitting a compressible fluid, either above or below the critical pressure ratio, provided that the corresponding value for incompressible flow, C_i, be known.

INTRODUCTION

When a fluid is discharged through a convergent nozzle, conditions across the exit section are generally assumed, with little error, to be sensibly uniform. The exit velocity may therefore be predicted from one-dimensional considerations, thus enabling the mass flow to be determined. This approach is not appropriate to the exit conditions across an orifice, since the streamlines are generally still contracting, so that the flow pattern is essentially two- or three-dimensional in character in this region. If, however, conditions may be assumed to be nearly uniform across some other section, such as at a *vena contracta* or at a throat, the principles of energy, momentum, and continuity may enable both the size of the jet and the conditions across it to be simply determined at this section.

Such principles, when applied to the discharge of an incompressible fluid through a Borda mouth-piece, for example, show that, if friction and gravity may be neglected, the jet has a contraction coefficient of 0·5. By the application of similar reasoning it will be shown that a theoretical expression for the contraction coefficient, C, may be determined, appropriate to an orifice when transmitting a compressible fluid, either above or below the critical pressure ratio, provided that the corresponding value for incompressible flow, C_i, be known.

Comparison with such experiments as those of Stanton (1926)†, Schiller (1933) and Perry (1949) indicates that the mass flow through a sharp-edged orifice may be predicted to within a few per cent at any pressure ratio. These tests were carried out on one type of orifice, transmitting either air or superheated steam, but the theory is more general in character, and further comparisons with tests are needed.

The present analysis considers cases in which the effect of friction is small, gravity and heat transfer may be neglected, and isentropic changes of state may be represented over the range considered by a law of the type:

$$p/\rho^n = \text{constant}$$

The above assumptions, which are adopted in most nozzle and orifice problems, are generally found in practice to give adequate accuracy, without making the analysis excessively tedious. The theory is divided into two parts; in the first, the pressure ratio across the orifice is assumed to be greater than the critical value, so that the flow is everywhere subsonic; in the second, choked flows are considered. The former case assumes constant conditions across the *vena contracta* which the jet may be expected ultimately to form, and the latter case makes a similar assumption concerning the first throat, where sonic conditions are postulated.

The contraction coefficient is defined as the ratio of the above minimum areas to the nominal projected area of the orifice (normal to the jet) and, since at the critical pressure ratio the *vena contracta* may be identified with the first throat, the two definitions are compatible for the borderline case dividing the two regimes. It is perhaps worth noting at this stage that although for supercritical conditions the flow is choked, in so far as conditions are sonic at the first throat, the mass flow does not become independent of the downstream pressure. This characteristic difference between the behaviour of the flow through a nozzle (which always flows full) as distinct from an orifice (through which contraction of the jet occurs), was noted and qualitatively explained by Stanton (1926), who indicated that the throat of the jet may be expected to increase in size as the back pressure is reduced.

By postulating, in addition, that compressibility effects may be neglected in the approach area to the orifice, quantitative expressions for these phenomena are deduced. Probably the most questionable of the above assumptions is that concerning conditions across the throat for supercritical flows, since the outermost layer must be at the back pressure. However, the curvature of the streamlines, which will be most marked towards the edge of the jet, implies a transverse pressure gradient in this region. This will give rise to a pressure distribution across the throat that is somewhat as indicated in Fig. 1.

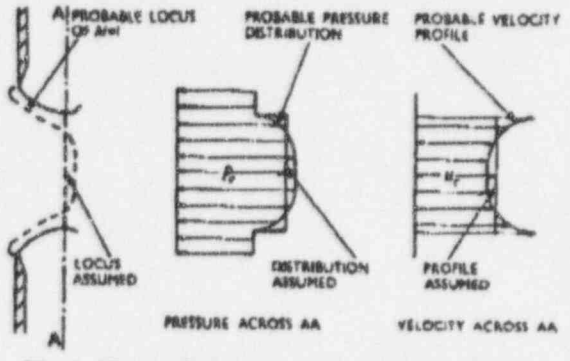

Fig. 1. Throat Conditions for Supercritical Flows

It is beyond the scope of a one-dimensional treatment to incorporate such refinements and, in the subsequent analysis, the throat will be assumed to be at the critical pressure. The error introduced by establishing the equation of motion on this basis will be largely offset by the corresponding assumption that the velocity is sonic across the whole section, whereas in practice it must be supersonic towards the edge of the jet, if the effect of viscosity is negligible. Since the latter factor must tend to retard the outer layers of the jet, some uncertainty, in any event, exists concerning conditions in this region.

Notation.

A	Projected area of orifice.
a	Contracted area of jet.
C	Contraction coefficient of orifice.
C_i	Contraction coefficient of orifice for incompressible flow.
C_v	Viscosity correction factor, $\dot{m}_a/\dot{m}$.
F	Force defect on reservoir walls.
f	Force defect coefficient.
g	Gravitational acceleration.
H	Total hydraulic head in reservoir.
K	Theoretical mass-flow coefficient of orifice.
K_N	Theoretical mass-flow coefficient of nozzle.
$\dot{m}$	Theoretical mass flow ($= W/g$).
$\dot{m}_a$	Actual mass flow.
n	Index of isentropic expansion ($= \gamma$ for a perfect gas).

The MS. of this paper was received at the Institution on 6th August 1954.

* Engineering Laboratory, Royal Naval College, Greenwich.

† An alphabetical list of references is given in Appendix II.

p_0 Pressure in reservoir.
p Back pressure.
r Pressure ratio, p/p_0.
r_c Critical pressure ratio.
u Velocity through contracted area.
u_c Critical velocity.
W Discharge, weight/time.
W_n Discharge through corresponding nozzle.
w_0 Specific weight in reservoir.
γ Ratio of specific heats, c_p/c_v.
ρ Density at contracted area.
ρ_0 Density in reservoir ($= w_0/g$).

SUBCRITICAL FLOW AND THE FORCE DEFECT COEFFICIENT

Suppose that a compressible fluid issues from a reservoir in which conditions are steady, through an orifice having a projected area, A, normal to the axis of the fluid jet, as indicated in Fig. 2*a*. By equating the resultant force acting on the fluid

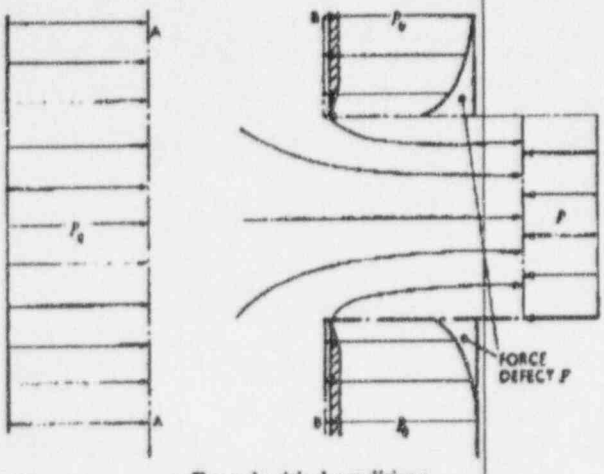

a For subcritical conditions.

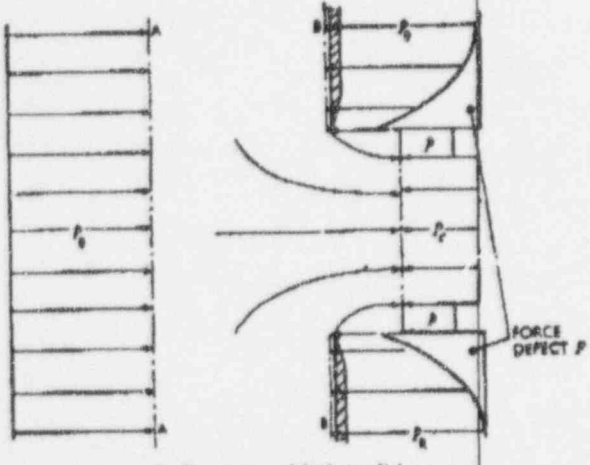

b For supercritical conditions.

Fig. 2. Forces on Control Volume

contained within the boundaries AA and BB to the corresponding flux of momentum through them, an equation of motion is obtained:

$$(p_0-p)A+F=\dot{m}u \quad . \quad . \quad . \quad . \quad . \quad (1)$$

The first term represents the direct driving force across the orifice area, and the second term the integral of the resolved components of the defects of pressure along the walls of the reservoir surrounding the aperture. This latter force defect, F, is associated with the velocity of the fluid as it approaches the orifice, the increase of kinetic energy occurring at the expense of its pressure energy. The tailing-off of pressure due to this sink effect adds to the driving force as indicated, enhancing the momentum flux through the boundaries.

For an orifice the fluid velocity will be comparatively small along the reservoir walls, and hence the effect of compressibility on the flow pattern actually within the reservoir may be neglected. This assumption will be increasingly valid as the orifice shape approaches that of a Borda mouth-piece from a nozzle-like form. If, however, the effect of compressibility on the force defect may be neglected, it should be possible to express it in terms of a Newtonian force coefficient which is a constant. That is, if the fluid may be assumed sensibly incompressible within the reservoir, the force defect, F, should be a unique function of the reservoir density ρ_0, the size of the orifice, as described by A for example, and the efflux, which is probably most conveniently expressed in terms of the mass flow, $\dot{m}$. This presupposes that the streamline pattern within the reservoir is not modified to any appreciable extent by changes in the boundary conditions downstream, associated with, for example, compressibility effects on the form of the emergent jet. If these assumptions are valid:

$$F=\phi(\dot{m}, A, \rho_0)$$

Dimensional considerations suggest that the relation between these variables must be of the form:

$$F=f\frac{\dot{m}^2}{\rho_0 A} \quad . \quad . \quad . \quad . \quad . \quad . \quad (2)$$

where f is a dimensionless coefficient having a value depending only on the form of the orifice. It will subsequently be referred to as the force defect coefficient. Since f may be expected to have the same value, whatever the Mach number of the flow, its value may be inferred from low-speed or incompressible-flow theory or tests. If the contraction coefficient of the orifice is denoted by C_i for incompressible flow, the corresponding volumetric flow rate:

$$Q=C_i A u \quad . \quad . \quad . \quad . \quad . \quad . \quad (3)$$

where u is the velocity of the contracted jet which, neglecting friction, is given by:

$$u=\sqrt{(2gH)}$$

This equation, when re-expressed in terms of the notation of the paper, becomes:

$$u=\sqrt{\frac{2(p_0-p)}{\rho_0}} \quad . \quad . \quad . \quad . \quad . \quad (4)$$

In practice, it is found that the resulting expression for the discharge requires factoring by a so-called coefficient of velocity to align theory with experiment, but at high Reynolds numbers the value of this coefficient is only slightly less than unity. Throughout the subsequent analysis of compressible flows the effect of friction will be neglected, it being recognized that the theoretical mass flow may require a correction for the effect of viscosity. This will be presumed to be of the same order as the velocity coefficient for incompressible flow.

Equation (3) may be re-expressed in terms of the mass flow as:

$$\dot{m}=\rho_0 C_i A u$$

and, when the theoretical expression for the velocity is substituted into this from equation (4), it becomes:

$$\dot{m}=\rho_0 C_i A\sqrt{\frac{2(p_0-p)}{\rho_0}}$$

These equations enable the first and last terms in the equation of motion (1) to be expressed for incompressible flow as:

$$(p_0-p)A=\frac{1}{2C_i^2}\cdot\frac{\dot{m}^2}{\rho_0 A}$$

$$\dot{m}u=\frac{1}{C_i}\cdot\frac{\dot{m}^2}{\rho_0 A}$$

On making these substitutions, together with that for the force defect given by equation (2), f is found to be uniquely related to C_i:

$$\frac{1}{2C_i^2}\cdot\frac{\dot{m}^2}{\rho_0 A}+f\cdot\frac{\dot{m}^2}{\rho_0 A}=\frac{1}{C_i}\cdot\frac{\dot{m}^2}{\rho_0 A}$$

that is,

$$f=\frac{1}{C_i}-\frac{1}{2C_i^2} \quad . \quad . \quad . \quad (5)$$

Since the incompressible-flow contraction coefficient lies between the values for a Borda mouth-piece, for which $C_i = 0{\cdot}5$, and for a nozzle, for which $C_i = 1$, it follows that the force defect coefficient will lie between the limits $0 < f < 0{\cdot}5$. That f is zero for a Borda mouth-piece might have been anticipated from physical considerations, since in this case the velocity along the walls of the reservoir tends to zero everywhere (except along the re-entrant portion, which gives rise to no additional force along the axis of the jet). The above expression for f provides the key to the remainder of the analysis since it has been argued that it may, with little error, be carried forward unchanged to an analysis of compressible flow through the orifice.

In order to use the equation of motion to determine the discharge for compressible flows in terms of f, which will now be presumed known, an expression is required for the velocity developed by the contracted jet. For the ideal case of a reversible adiabatic expansion, the Saint-Venant and Wanzel equation is appropriate, and this is, for subcritical flows:

$$u = \sqrt{\left\{\frac{p_0}{\rho_0}\cdot\frac{2n}{n-1}\cdot\left(1-r^{\frac{n-1}{n}}\right)\right\}} \quad . \quad . \quad . \quad (6)$$

where r denotes the pressure ratio, p/p_0, and n is the index which best represents isentropic expansions by a law of the type:

$$p/\rho^n = \text{constant}$$

For a near-perfect gas n may, of course, be identified with γ, the ratio of the specific heats. If the contraction coefficient be denoted by C, the mass flow is then:

$$\dot{m} = \rho C A u$$

$$= CA\sqrt{\left\{p_0\rho_0\frac{2n}{n-1}\cdot r^{2/n}\cdot\left(1-r^{\frac{n-1}{n}}\right)\right\}} \quad . \quad (7)$$

By substituting the value $C = 1$ the corresponding widely used expression for a nozzle is obtained. This suggests that the corresponding mass-flow coefficient for a nozzle, K_N, may be used as a convenient substitution:

$$K_N = \sqrt{\left\{\frac{2n}{n-1}r^{2/n}\left(1-r^{\frac{n-1}{n}}\right)\right\}} \quad . \quad . \quad . \quad (8)$$

Hence, for a nozzle:

$$\dot{m} = K_N A\sqrt{(p_0\rho_0)}$$

and, for an orifice,

$$\dot{m} = CK_N A\sqrt{(p_0\rho_0)} \quad . \quad . \quad . \quad . \quad . \quad . \quad . \quad . \quad (9)$$

The velocity through the contracted area of the jet is, in either case, given by equation (6) which on substituting for K_N reduces to:

$$u = \frac{K_N}{r^{1/n}}\sqrt{\frac{p_0}{\rho_0}} \quad . \quad . \quad . \quad . \quad . \quad . \quad . \quad (10)$$

Hence, for subcritical compressible flows, the last term in the equation of motion (1) for an orifice becomes:

$$\dot{m}u = \frac{C(K_N)^2 A p_0}{r^{1/n}}$$

The force defect may similarly be expressed in terms of K_N as:

$$F = f\cdot\dot{m}^2/\rho_0 A$$

$$= fC^2(K_N)^2 A p_0$$

so that the equation of motion gives, with those substitutions, a quadratic expression for C:

$$(1-r)Ap_0 + fC^2(K_N)^2 Ap_0 = \frac{C(K_N)^2 Ap_0}{r^{1/n}}$$

that is,

$$fC^2 - \frac{1}{r^{1/n}}C + \frac{1-r}{(K_N)^2} = 0$$

Therefore

$$C = \frac{1}{2fr^{1/n}}\left[1-\sqrt{\left\{1-\frac{(2r^{1/n})^2(1-r)f}{(K_N)^2}\right\}}\right] \quad . \quad . \quad (11)$$

Since it will be noted that K_N depends only on r and n, the contraction coefficient is thus determined for subcritical flows as a function of r, n, and f, the latter being found from the incompressible-flow contraction coefficient, C_i.

The theoretical mass flow may then be deduced by factoring the Saint-Venant and Wanzel equation for the mass flow by the contraction coefficient. It remains to develop an expression corresponding with equation (11), to cover those cases in which the local Mach number reaches unity in the jet. Such flows, which will be referred to as supercritical, are investigated in the next section.

SUPERCRITICAL FLOWS

It has been assumed above that the flow was both reversible and adiabatic during its expansion between the reservoir and the downstream pressures. This implied that friction and heat transfer could be neglected, and experiments with real fluids support this assumption for high-speed compressible flows. If, however, the downstream pressure is less than a certain critical pressure, p_c, so that the stream may become supersonic, the assumption of isentropic flow cannot be valid *a priori*, even though the flow be both frictionless and thermally insulated. This is due to the fact that shock waves may form as the fluid recompresses after over-expanding downstream of the first throat. Evidence of this alternative expansion and compression is provided by schlieren and shadowgraph photographs of fluid jets, and these wave phenomena might also be foreseen from theoretical considerations (for example, Stanton 1926).

It is therefore preferable to analyse supercritical flows in terms of a reference section across the first throat, rather than one across the section at which the fluid has expanded to the downstream pressure. This corresponds to the use of the throat as the control section in convergent–divergent nozzle problems, where conditions at exit are examined subsequently. The equations of motion will therefore be established in terms of the boundaries indicated in Fig. 2*b*. The pressure and velocity across the jet are considered to have values corresponding to sonic conditions. If these critical values are denoted by suffix c the equation of motion is:

$$p_0 A - pA(1-C) - p_c CA + F = \dot{m}u_c$$

The left-hand side of this equation consists of the direct driving force across the area of the orifice, together with the force defect, as before. In this case, however, although the force on boundary AA is unchanged, the back pressure across the area of the orifice, A, is now considered to consist of two parts, the critical pressure, p_c, being assumed to act across the throat area ($a = CA$) and the downstream pressure, p, to act over the area remaining.

For supercritical conditions the expressions for the throat velocity and mass flow are obtained by substituting the critical value of the pressure ratio into equations (6) and (7), as for a choked nozzle:

$$u_c = \sqrt{\left\{\frac{p_0}{\rho_0}\cdot\frac{2n}{n-1}\cdot\left(1-r_c^{\frac{n-1}{n}}\right)\right\}} = \sqrt{\left\{\frac{p_0}{\rho_0}\cdot\frac{2n}{n+1}\right\}}$$

$$\dot{m} = CA\sqrt{\left\{p_0\rho_0\cdot\frac{2n}{n-1}\cdot r_c^{2/n}\cdot\left(1-r_c^{\frac{n-1}{n}}\right)\right\}}$$

$$= CA\sqrt{\left\{p_0\rho_0\left(\frac{2}{n+1}\right)^{\frac{n+1}{n-1}}\right\}}$$

since $r_c = \left(\frac{2}{n+1}\right)^{\frac{n}{n-1}}$

If the substitution K_N is introduced as before to denote the mass-flow coefficient of the corresponding nozzle which, being choked, has the value:

$$K_N = \sqrt{\left\{\frac{2n}{n-1}\cdot r_c^{2/n}\left(1-r_c^{\frac{n-1}{n}}\right)\right\}} = \sqrt{\left\{n\left(\frac{2}{n+1}\right)^{\frac{n+1}{n-1}}\right\}} \quad (12)$$

the expressions for u_c and $\dot{m}$ become:

$$u_c = \frac{K_N}{r_c^{1/n}}\sqrt{\frac{p_0}{\rho_0}} \quad . \quad . \quad . \quad . \quad . \quad . \quad (13)$$

$$\dot{m} = CK_N A\sqrt{(p_0\rho_0)} \quad . \quad . \quad . \quad . \quad (14)$$

These equations are analogous to equations (9) and (10) although in this case r is replaced by the constant value r_c so that K_N is now independent of the pressure ratio r. The flux of momentum and the force defect may now be expressed as:

$$\dot{m}u_c = \frac{C(K_N)^2 A p_0}{r_c^{1/n}}$$

$$F = fC^2(K_N)^2 Ap_0$$

so that the equation of motion for choked flows is:

$$(1-r)Ap_0+(r-r_c)CAp_0+fC^2(K_n)^2Ap_0 = \frac{C(K_n)^2Ap_0}{r_c^{1/n}}$$

This again yields a quadratic expression for C:

$$fC^2-\frac{1}{r_c^{1/n}}\left[1+\frac{(r_c-r)r_c^{1/n}}{(K_n)^2}\right]C+\frac{1-r}{(K_n)^2} = 0$$

Therefore

$$C = \frac{1}{2fr_c^{1/n}}\left[\left\{1+\frac{(r_c-r)r_c^{1/n}}{(K_n)^2}\right\} - \sqrt{\left\{\left(1+\frac{(r_c-r)r_c^{1/n}}{(K_n)^2}\right)-\left(\frac{(2r_c^{1/n})^2(1-r)f}{(K_n)^2}\right)\right\}}\right] \quad . \quad . \quad . \quad (15)$$

This expression, which determines the contraction coefficient of a choked orifice, is seen to reduce to equation (11) when the overall pressure ratio, r, is equal to the critical value, r_c. The two equations together determine the contraction coefficient throughout the whole range of pressure ratios. The basic assumption is that the effect of compressibility on the force defect along the reservoir walls may be neglected; this may be expected to be valid so long as the orifice does not approach a nozzle form. For a Borda mouth-piece the force defect is zero and in this case the theory is, in this sense, exact. For such a mouth-piece it is convenient to return to the original quadratic expressions for C, since these reduce to linear equations in the limiting case when f is zero. For a Borda mouth-piece the expressions for its contraction coefficient, C_b, thus reduce to:

$$C_b = \frac{r^{1/n}(1-r)}{(K_n)^2} \quad . \quad . \quad . \quad . \quad . \quad (16)$$

for subcritical flows, that is, when $r_c<r<1$, and

$$C_b = \frac{r_c^{1/n}(1-r)}{r_c^{1/n}(r_c-r)+(K_n)^2} \quad . \quad . \quad . \quad (17)$$

for choked flows, that is, when $0<r<r_c$.

By substituting the choked value of K_n from equation (12) in equation (17), the latter may be expressed more simply, after some algebraic manipulation, as:

$$C_b = \frac{1-r}{r_c(1+n)-r}$$

This theoretical expression presupposes that the mouth-piece is short enough for the emergent jet to clear the outer lip of the orifice, although, of course, not so short that there is an appreciable approach velocity along the reservoir wall.

SUMMARY AND THEORETICAL CURVES

The purpose of the paper is to present a method of finding the discharge through any orifice, when transmitting a compressible fluid, either above or below the critical pressure ratio.

It is presumed that the incompressible-flow contraction coefficient, C_i, is known either from theory or experiment; for example, $C_i = 0{\cdot}5$ for a Borda mouth-piece and $C_i = \pi/(\pi+2) = 0{\cdot}611$ for a plane slit. From C_i the strength of the sink effect along the reservoir walls may be inferred. Its intensity determines the magnitude of a force defect coefficient, f, such that:

$$f = \frac{1}{C_i}-\frac{1}{2C_i^2}$$

On the assumption that the flow pattern within the reservoir is very little influenced by the effect of compressibility, f enables theoretical expressions for the contraction coefficient, C, to be deduced for compressible flows, both above and below the critical pressure ratio. This contraction coefficient enables the mass flow to be determined from the expression:

$$\dot{m} = CK_nA\sqrt{(p_0\rho_0)}$$

For a nozzle $C = 1$, and hence K_n is the widely used mass-flow coefficient for a nozzle, based on the Saint-Venant and Wanzel equation. This mass-flow coefficient is shown dotted in Fig. 3 for the typical case of $n = 1{\cdot}4$. The contraction coefficient at any particular pressure ratio may be found by first determining f and K_n and substituting their values into either equation (11) or equation (15) according to whether r is greater or less than the critical value r_c. Some representative curves have been obtained in this way and plotted in Fig. 4. They indicate that, as the back pressure is reduced, the jet expands progressively, thus causing a continuous increase in the flow rate. This process continues into the supercritical flow range (although at a decreasing rate) so that even though the flow is choked, in the sense that conditions at the throat remain constant, the mass flow continues to increase. This fact is emphasized by defining a theoretical mass-flow coefficient for an orifice K such that:

$$K = CK_n = \frac{\dot{m}}{A\sqrt{(p_0\rho_0)}}$$

Curves showing the theoretical variation of K with pressure ratio have been plotted in Fig. 3, which includes the corresponding curve for a nozzle (K_n). Comparison of the orifice

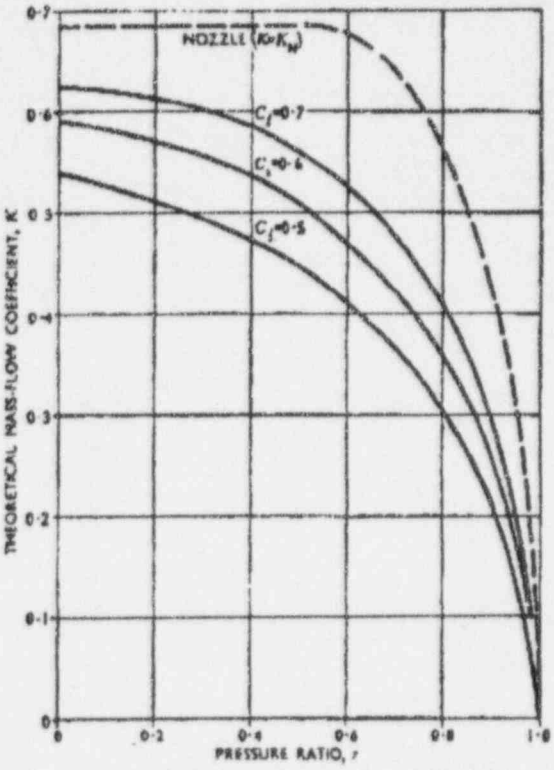

Fig. 3. Theoretical Mass-flow Coefficient Plotted as a Function of Pressure Ratio for $n = 1{\cdot}4$

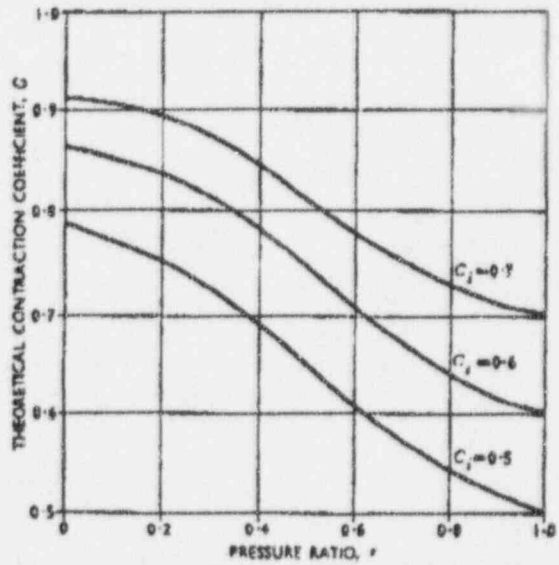

Fig. 4. Theoretical Contraction Coefficient Plotted as a Function of Pressure Ratio for $n = 1{\cdot}4$

and nozzle curves indicates the characteristic difference between their behaviour, the choking of the former being completely masked by the variation of C with r. A numerical example is given in Appendix I.

COMPARISON WITH THE HODOGRAPH SOLUTION FOR A PLANE SLIT

Theoretical results for incompressible flow through orifices can, under certain conditions, be extended to compressible flows, using a hodograph method (Howarth 1953). The results shown in Table 1 for the contraction coefficient of a slit in a plane wall

TABLE 1. CONTRACTION COEFFICIENT OF SLIT IN PLANE WALL

r	C
1·000	0·611
0·932	0·623
0·867	0·636
0·805	0·650
0·747	0·665
0·692	0·681
0·639	0·699
0·590	0·717
0·543	0·738
0·528	0·745

have been computed, using tables due to Ferguson and Lighthill (1947).

The results in Table 1 are appropriate to $\gamma = 1{\cdot}4$ and the method applies to subsonic flows only ($r > 0{\cdot}528$).

The corresponding values obtained by the method outlined in the paper are as given in Table 2, at roughly comparable

TABLE 2. CORRESPONDING VALUES FOR CONTRACTION COEFFICIENT OBTAINED BY METHOD OUTLINED IN THE PAPER

r	C	Error
1·00	0·611	—
0·932	0·622	−0·001
0·865	0·635	−0·001
0·805	0·648	−0·002
0·745	0·663	−0·002
0·690	0·679	−0·002
0·640	0·696	−0·003
0·590	0·714	−0·003
0·545	0·734	−0·004
0·528	0·741	−0·004

values of r, together with the 'error' treating the hodograph solution as 'exact'.

It can be seen that the present method slightly underestimates the mass flow, the discrepancy increasing progressively from zero to about 0·5 per cent at the critical pressure ratio.

COMPARISON WITH EXPERIMENT, AND CONCLUSIONS

Probably the most exhaustively tested orifice is that of the sharp-edged type. The results of Perry (1949) and Schiller (1933) using such an orifice to transmit air and steam, respectively, have been plotted in Fig. 5*a* and *b*. Since the incompressible-flow discharge coefficient is considered to be 0·6 in each instance, this corresponds to a velocity coefficient, as used in hydraulics, of 0·982, if the contraction coefficient be given the datum value of 0·611. It would appear logical to retain the correction factor C_v for the theoretical curves throughout the range of pressure ratios. The actual mass flow for a real fluid, $\dot{m}_a$, is then predicted by:

$$\frac{\dot{m}_a}{A\sqrt{(p_0\rho_0)}} = C_v C K_M = C_v K$$

It is perhaps preferable to consider C_v in the general case as an overall correction for viscosity effects, rather than simply as a velocity coefficient. In Fig. 5*a* and *b* the theoretical curves have been drawn, both with and without the factor $C_v = 0{\cdot}982$. It is seen that the experimental results in each instance lie between the two curves, making it problematic as to whether such a correction is worth while. In either instance the agreement appears satisfactory for most purposes for sharp-edged orifices transmitting either air or steam.

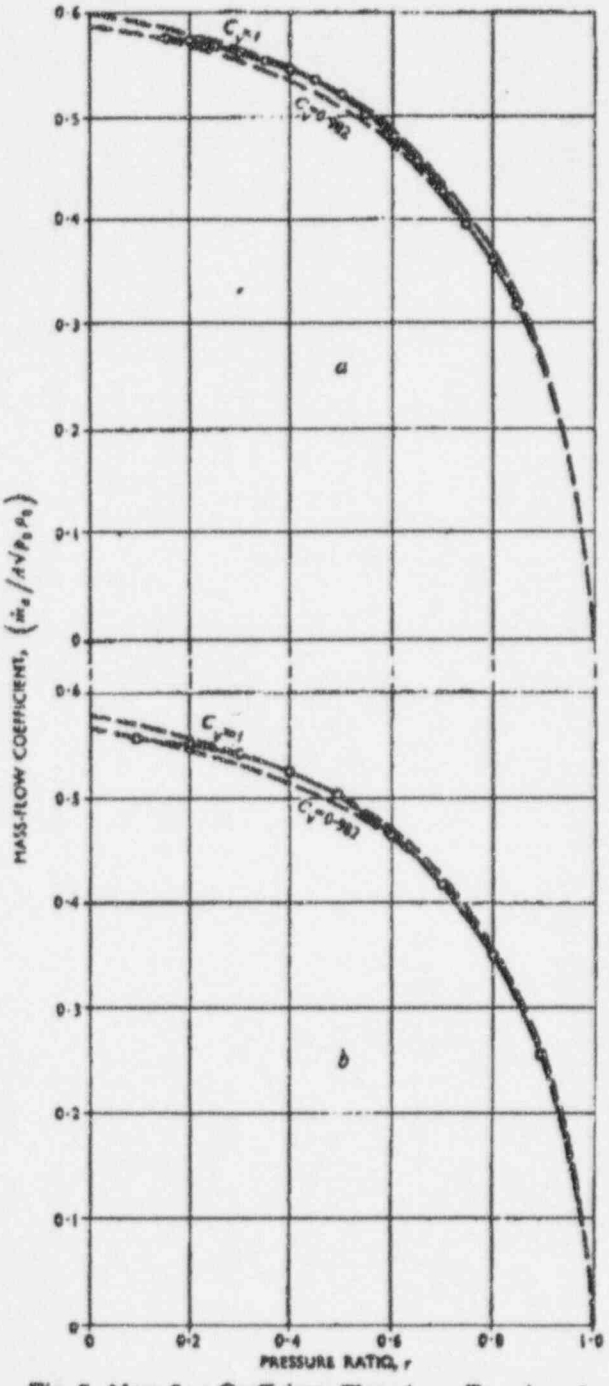

Fig. 5. Mass-flow Coefficients Plotted as a Function of Pressure Ratio

a For $n = 1{\cdot}4$.
——○—— Perry's tests, using air.
— — — — Theory ($n = 1{\cdot}4$, $C_i = r/(r+2)$).

b For $n = 1{\cdot}3$.
——○—— Schiller's tests, using steam.
— — — — Theory ($n = 1{\cdot}3$, $C_i = r/(r+2)$).

Further comparisons of the theory with experiment are required to establish the full range over which the assumptions of the theory are valid. Since the neglect of compressibility within the reservoir cannot be justified when the orifice tends to a nozzle-like form, an upper limit of $C_i = 0{\cdot}7$ for application of the theory is tentatively suggested.

ACKNOWLEDGEMENT

The author's thanks are due to the staff of the Aerodynamics Department of the Royal Aircraft Establishment, Farnborough, for their advice and criticism during the preparation of the paper. It is published by permission of the Admiralty, but the views expressed are personal to the author.

APPENDIX I*

NUMERICAL EXAMPLE

Many engineers prefer to work in terms of the weight flow, W, and specific weight, w, rather than the mass flow, $\dot{m}$, and density, ρ, to which they are related by:

$$W = \dot{m}g$$
$$w = \rho g$$

From equation (9) the discharge in terms of W becomes:

$$W = CK_N A g\sqrt{(p_0\rho_0)}$$

that is,

$$W = CK_N A\sqrt{(gp_0w_0)} \quad . \quad . \quad . \quad (18)$$

For a nozzle $C = 1$, so that the corresponding nozzle discharge is:

$$W_N = K_N A\sqrt{(gp_0w_0)} \quad . \quad . \quad . \quad (19)$$

A number of methods, using charts, tables, or working rules, have been developed by engineers for calculating W_N. As a typical example may be quoted Napier's equation for a choked nozzle discharging steam:

$$W_N = Ap_0/70 \quad . \quad . \quad . \quad . \quad (20)$$

in which W_N is the discharge in Lb. per sec; A is the throat area in in^2; and p_0 is the reservoir pressure in Lb/in^2.

The discharge through an orifice is related to the corresponding nozzle discharge by:

$$W = CW_N \quad . \quad . \quad . \quad . \quad . \quad (21)$$

C is the contraction coefficient, which may be obtained from Fig. 4 for a specified pressure ratio, r, and incompressible-flow contraction coefficient, C_i, as used in hydraulics. Fig. 4 refers strictly to an expansion index $n = 1{\cdot}4$, but the value of C does not appear to be critically dependent on n. The corresponding algebraic expressions for C are equations (11) and (15) for subcritical and choked flows, respectively. In the former expression K_N is given by equation (8) and in the latter by equation (12). If the equivalent nozzle discharge has been determined without reference to these equations, K_N may alternatively be deduced from W_N by use of equation (19).

As a typical numerical example the leakage rate through an annular slit which is 6 inches in diameter and 0·01 inch wide will be estimated. It has an area:

$$A = \pi \times 6 \text{ in} \times 0{\cdot}01 \text{ in} = 0{\cdot}1885 \text{ in}^2$$

and, if it were one stage of a labryrinth seal, for example, it would probably have a hydraulic (that is, incompressible-flow) contraction coefficient, $C_i = 0{\cdot}6$. Thus the corresponding force defect coefficient is, by equation (5):

$$f = \frac{1}{C_i} - \frac{1}{2C_i^2}$$
$$= \frac{1}{0{\cdot}6} - \frac{1}{2\times 0{\cdot}6^2} = 0{\cdot}278$$

* The nomenclature used in this appendix was adopted at the special request of the author.

Neglecting any velocity of approach or 'carry over' effects, the nozzle mass-flow coefficient is, for subcritical flows:

$$K_N = \sqrt{\left\{\frac{2n}{n-1}r^{2/n}\left(1 - r^{\frac{n-1}{n}}\right)\right\}}$$

For superheated steam at the critical pressure ratio ($r = r_c = 0{\cdot}546$, if $n = 1{\cdot}3$):

$$K_N = 0{\cdot}667$$

For values of r less than 0·546, K_N remains constant at this value.

Suppose that the discharge corresponding to a pressure ratio of 0·546 is required. From equation (8) (or equation (12)):

$$C = \frac{1}{2fr^{1/n}}\left[1 - \sqrt{\left\{1 - \frac{(2r^{1/n})^2(1-r)f}{(K_N)^2}\right\}}\right]$$
$$= \frac{1}{2\times 0{\cdot}278\times 0{\cdot}546^{\frac{1}{1{\cdot}3}}} \times$$
$$\left[1 - \sqrt{\left\{1 - \frac{\left(2\times 0{\cdot}546^{\frac{1}{1{\cdot}3}}\right)^2 \times 0{\cdot}454 \times 0{\cdot}278}{0{\cdot}667^2}\right\}}\right]$$
$$= 2{\cdot}865[1 - 0{\cdot}744]$$
$$= 0{\cdot}732$$

The equivalent nozzle discharge may be obtained from:

$$W_N = K_N A\sqrt{(gp_0w_0)}$$

or by any other preferred method. If the steam is initially at, for example, 200 Lb/in^2 and has 100 °F of superheat, its total heat, or enthalpy, is 1,258 B.t.u./Lb. Its corresponding specific volume is thus, according to Callendar (1939):

$$\frac{1}{w_0} = 1{\cdot}253 \times \frac{1{,}258 - 835}{200} \text{ ft}^3/\text{Lb}$$

that is, $w_0 = 0{\cdot}377$ Lb/ft^3

Therefore,

$$W_N = 0{\cdot}667 \times 0{\cdot}1885 \text{ in}^2 \sqrt{(32{\cdot}2 \text{ ft/sec}^2}$$
$$\times 200 \text{ Lb/in}^2 \times 0{\cdot}377 \text{ Lb/ft}^3)[1 \text{ ft}/12 \text{ in}]$$
$$= 0{\cdot}516 \text{ Lb/sec}$$

Hence, the discharge through the orifice is, finally:

$$W = CW_N$$
$$= 0{\cdot}732 \times 0{\cdot}516 \text{ Lb/sec}$$
$$= 0{\cdot}378 \text{ Lb/sec}$$

This flow rate corresponds with a reservoir pressure of 200 Lb/in^2 and a back pressure of $0{\cdot}546 \times 200$ Lb/in^2 that is, 109 Lb/in^2. Any reduction in the latter does not affect W_N but it does increase C, thus increasing the discharge, W, even though the orifice is choked.

APPENDIX II

REFERENCES

CALLENDAR, H. L. 1939 'Abridged Callendar Steam Tables, Fahrenheit Units' (Edward Arnold and Co.).

FERGUSON, D. F., and LIGHTHILL, M. J. 1947 Proc. Roy. Soc., vol. A192, p. 135, 'The Hodograph Transformation in Trans-sonic Flow'.

HOWARTH, E. L. 1953 'Modern Developments in Fluid Dynamics: High Speed Flow', vol. 1, p. 222 (Oxford University Press).

PERRY, J. A., jun. 1949 Trans. A.S.M.E., vol. 71, p. 757, 'Critical Flow Through Sharp-edged Orifices'.

SCHILLER, W. 1933 *Forschung auf dem Gebiete des Ingenieurwesens*, vol. 4, p. 128, 'Überkritische Entspannung kompressibler Flüssigkeiten'.

STANTON, T. E. 1926 Proc. Roy. Soc., vol. A111, p. 306, 'The Flow of Gases at High Speeds'.

Communications

Mr. C. H. Bosanquet (Billingham) wrote that the author's method of calculating discharge coefficients depended entirely on the assumption of the constancy of f, using his formula

$$\frac{dC}{df} = \frac{C^3}{1-C}$$

Values of C approaching unity must therefore be very sensitive to small variations of f.

For a perfect nozzle $C = 1$ by definition but if $f = 0{\cdot}5$ and $n = 1{\cdot}4$ then C, which was initially unity, fell rapidly with decreasing r and passed through a minimum value of 0·852 when $r = 0{\cdot}7$. It then rose to 0·888 at the critical ratio and 0·959 for discharge into a vacuum.

If C was assumed constant then $f = 0{\cdot}5$ for small pressure differences and rose to 0·571 at and beyond the critical ratio.

For intermediate conditions it varied nearly linearly with pu^2.

Critical data for other values of n were given in Table 3.

Table 3. Critical Data for Various Values of n

n	r_c	f_c/f_0
1·0	0·6065	1·1584
1·1	0·5847	1·1541
1·2	0·5645	1·1500
1·3	0·5457	1·1462
1·4	0·5283	1·1427
1·667	0·4871	1·1341

A suggested modification of the method was to multiply f_0 by a factor which depended on the mean mass flow in the plane of the orifice. The modified value of f was given by

$$\frac{f}{f_0} = 1 + \left(\frac{f_c}{f_0} - 1\right)\frac{\rho_c}{\rho}\left(\frac{\rho u}{\rho_c u_c}\right)^2$$

Densities and velocities were assumed the same as for a nozzle with the same mass flow. The value of ρu in the orifice plane depended on C so that it was necessary to solve by trial. The calculation of f was facilitated by employing the useful and adequately accurate approximation

$$\left(\frac{\rho u}{\rho_c u_c}\right)^2 + \left(\frac{r - r_c}{1 - r_c}\right)^2 = 1$$

At and beyond the critical ratio the first term was simply equal to C^2.

Table 1 gave values which fell almost exactly half-way between those calculated by the two methods so that the comparison was inconclusive. For small discharge coefficients and subsonic flows the modification did not make much difference. For values of C approaching unity the modified method gave results which were at least possible; constant f did not. The modified method therefore appeared preferable in spite of its greater complexity.

Mr. R. P. Fraser and Dr. P. N. Rowe (London) wrote that as a result of experimental work carried out in the High Speed Fluid Kinetics Laboratory of the Imperial College of Science and Technology (Fraser and Rowe 1954*, Coulter, Fraser, and Rowe (to be published)†, and Coulter 1949‡) it was possible to contribute some data to compare with the theoretical predictions of the paper in the supersonic range.

Since a velocity coefficient of 1·00 was assumed, the contraction coefficient referred to in the paper was equivalent to a discharge coefficient. They had measured the discharge coefficient of various nozzles discharging air at pressure ratios from r equal to 0·012 to 0·033. All the nozzles had a throat of a nominal diameter of $\frac{1}{2}$ inch. Comparative discharge coefficients for various nozzles had been obtained by timing the rate of fall of reservoir pressure under similar conditions.

Fig. 6 showed the effect of the entry radius on the discharge coefficient of a supersonic convergent-divergent nozzle. Since the stream was everywhere supersonic downstream of the throat, it could not influence conditions upstream. In other words, in any supersonic nozzle the upstream flow was unaffected by the divergent section and, in particular, the discharge coefficient was unaltered by the supersonic expansion section. That was indeed

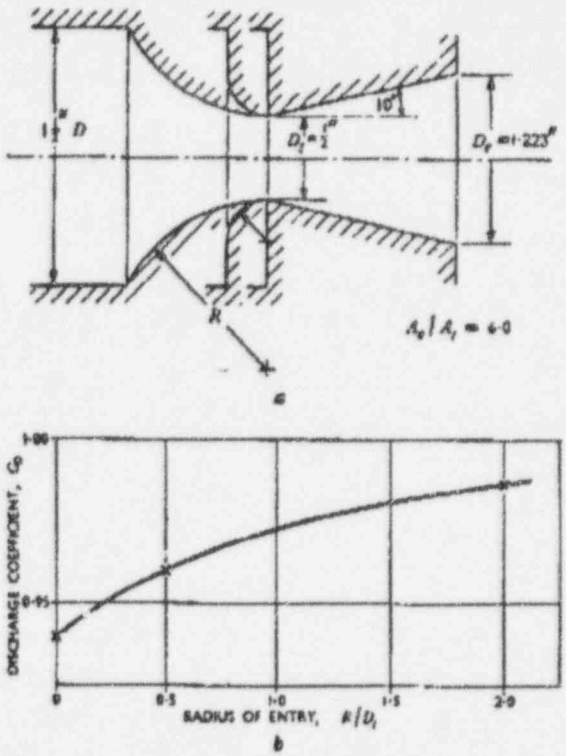

Fig. 6. Effect of Entry Radius on Discharge Coefficient of Supersonic Convergent-divergent Nozzle

R/D	0	0·5	2·0
C_D	0·939	0·960	0·986

the case in practice for experiments had shown that the discharge coefficient was independent of the divergent section within the limits of experimental error (±0·01). Thus, the nozzle with $R/D_t = 0$ was, in the supersonic (i.e., the author's supercritical) region, equivalent to an orifice where $C_i = 0{\cdot}6$. One with $R/D_t = 2{\cdot}0$ corresponded to a nozzle where $C_i = 1{\cdot}0$. The author had predicted a difference in discharge coefficient between those two nozzles of about 0·14 (Fig. 4) whereas they had found 0·047. However, an increased contraction coefficient for incompressible flow (which they had not measured) would bring those results more into line.

* Fraser, R. P., and Rowe, P. N. 1954 Jl. of the Imperial College Chem. Eng. Soc., vol. 8, p. 1, 'A Method of Measuring Very Large Gas Flow Rates'.

† Coulter, M. O., Fraser, R. P., and Rowe, P. N. (to be published), 'A Research into the Design of Supersonic Nozzles for Rockets'.

‡ Coulter, M. O. 1949 Ph.D. Thesis, London University, June, 'On the Efficiency of Supersonic Nozzles'.

In addition to measuring the discharge coefficient, they had measured the thrust reaction generated by the jets from various nozzles. Since the thrust was proportional to the product of discharge rate and the acceleration occurring in the nozzle, the thrust coefficient was equal to the product of discharge coefficient and velocity coefficient. For the case of a convergent-divergent nozzle cut off at the throat (i.e., without a supersonic expansion section), the velocity coefficient corresponded to that of the author which he had assumed to be unity.

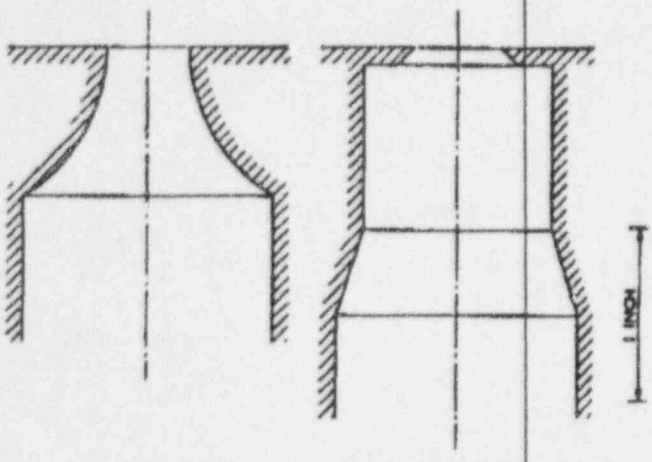

a Radiused nozzle. *b* Orifice with modified approach.

Fig. 7. Two Nozzles

Thrust measurements made on the two nozzles of Fig. 7 showed that the thrust coefficient for that with the radiused approach ($R/D_t = 2{\cdot}0$) was 0·975 and that for the orifice with a modified approach was 0·908 (±0·007). (Unfortunately they had no data for the conventional orifice treated in the paper.) The discharge coefficient for the radiused nozzle was known from the data of Fig. 6 (0·986) and so its velocity coefficient was 0·975/0·986 = 0·989 which justified the author's assumption, in that instance, that the velocity coefficient was unity. If for the orifice with the modified approach the discharge coefficient for a nozzle of $R/D_t = 0$ was used (0·939), the velocity coefficient for that was 0·908/0·0939 = 0·967 so that in that instance the assumption of a velocity coefficient of unity was much less accurate.

The author appeared to have assumed that there was a *vena contracta* in compressible flow at small pressure ratios (i.e. high reservoir pressures). Expansion at the exit plane according to the Prandtl–Meyer theory would produce immediate divergence as

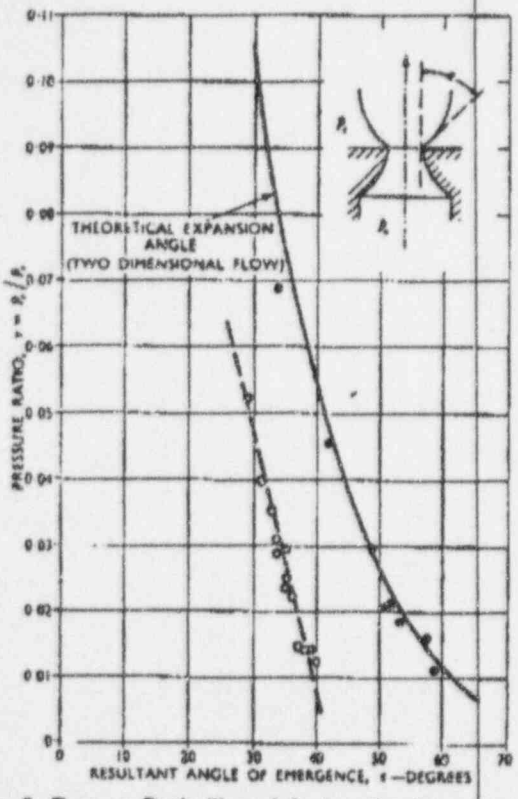

Fig. 8. Pressure Ratio Plotted Against Resultant Angle of Emergence

● Experimental points for radiused nozzle.
○ Experimental points for orifice with modified approach.

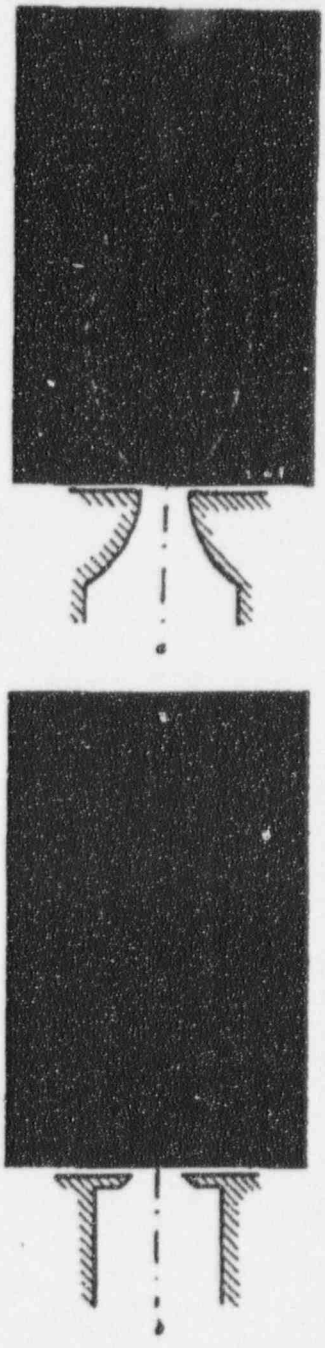

Fig. 9. Shadow Photographs
$r = 0{\cdot}024$.

shown in Fig. 8, in which the full line showed the theoretical expansion angle that would result from flow through a nozzle subjected to a pressure ratio, r. The treatment was for two-dimensional flow, $\gamma = 1{\cdot}40$, and it was assumed that the flow approached the throat perpendicularly. Those angles were achieved in practice for the three-dimensional flow of air through a radiused nozzle at different pressure ratios as was seen from the shadow photograph in Fig. 9*a*. The emergence angle had been measured from photographs of the jet at different pressure ratios and, for a radiused nozzle, they agreed closely with the theoretical angle as would be seen in Fig. 8.

Unfortunately, in the standard orifice the throat plane was not normally visible, which prevented photographic determination of the emergence angle. For the orifice with a modified approach, it would be seen that the emergence angle had been reduced (Figs. 8 and 9*b*) because the fluid now had radial velocity directed towards its flow axis which produced a contracting effect. That was precisely the effect the author had been considering but the result was a net enlargement, not a contraction.

The emergence angles for their orifice indicated a reduction of the Prandtl–Meyer angle. Thus, a parallel jet would emerge at some pressure ratio and at higher ratios the jet might contract outside the nozzle and the sonic plane would move downstream. Fig. 10 showed that a substantially parallel jet emerged at a pressure ratio of about 0·13 and that above that pressure ratio contraction occurred. It was not possible to measure those emergence angles very accurately but, undoubtedly, the order of the effect was as they had suggested.

They were of the opinion that the author's theoretical treatment must be modified for supersonic flow, particularly at high reservoir pressures, to take into account the expansion effect. They hoped in the near future to publish a comprehensive account of their experimental work in that field (Coulter, Fraser, and Rowe (to be published)).

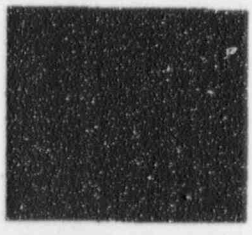

a For radiused nozzle with $r = 0{\cdot}23$.

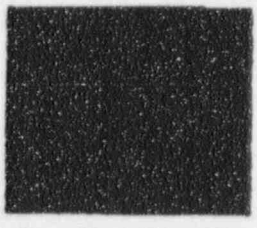

b For orifice with modified approach and $r = 0{\cdot}23$.

c For radiused nozzle with $r = 0{\cdot}13$.

d For orifice with modified approach and $r = 0{\cdot}13$.

Fig. 10. Emergence of a Substantially Parallel Jet

Mr. D. H. TANTAM (*Associate Member*) wrote that the mass flow of a compressible fluid through an orifice had been given in equation (7) as

$$m = CA\sqrt{\left\{p_0\rho_0\frac{2n}{n-1}\cdot r^{2/n}\cdot\left(1-r^{\frac{n-1}{n}}\right)\right\}}$$

In that an infinitely large reservoir to orifice area ratio was considered.

Many applications were concerned with an orifice in a pipeline when the ratio was much smaller and an equation which took that into account was given by

$$Q = \Omega A_2\left[\frac{2gp_1W_1\frac{\gamma}{\gamma-1}\left\{1-\left(\frac{p_2}{p_1}\right)^{\frac{\gamma-1}{\gamma}}\right\}\left\{\frac{p_2}{p_1}\right\}^{\frac{2}{\gamma}}}{1-\frac{1}{n^2}\left(\frac{p_2}{p_1}\right)^{\frac{2}{\gamma}}}\right]^{\frac{1}{2}}$$

where Q was the mass flow; Ω, the coefficient of discharge; A_2, the area of orifice; n, the ratio of area of pipeline to area of orifice; p_1, the upstream pressure; p_2, the downstream pressure; W_1, the specific weight of fluid; γ, the ratio of specific heats; and g, the acceleration due to gravity.

Equation (7) was obtained from it of course when $n = \infty$.

However, in the practical application, the mass flow would depend on the contraction coefficient C, theoretical values of which had been given in Fig. 4. He would like to know, however, whether any recent information had been established on those coefficients in addition to the work of Perry (1949) and Schiller (1933) and how those results agreed with theoretical values.

Author's Reply

Mr. D. A. JOBSON wrote, in reply to the communications, that he agreed that the force defect coefficient f could not, in general, be considered to be a constant. It was, in some respects, similar to a drag coefficient; just as the latter would depend on the Mach number, so f depended on the mass-flow coefficient and, hence, the pressure ratio r. It was only for orifice-like openings that the influence of compressibility on f might be expected to be small. The Borda mouth-piece represented one extreme for which f was always zero, whatever the value of r. At the other end of the scale, as Mr. Bosanquet had pointed out, f for a nozzle varied almost linearly with r from f_0 equal to 0·5 to the typical value of f equal to 0·571 for n equal to 1·4, thereafter it remained constant for choked flows. Hence the ratio f/f_0 might always be expected to lie between the limits of 1·0 and 1·14 for that value of n, and it could therefore always be estimated with reasonable certainty by some such method as he had suggested. That would enable the theory to be applied beyond the limit C_c equal to 0·7 which he himself had suggested, but he doubted whether the added complication was justifiable below that value.

He noted that Mr. Fraser and Dr. Rowe had measured discharges on an orifice fitted with an exit cone, which discharges were somewhat higher than those obtained and predicted for a simple orifice. It was his own belief that that interesting anomaly might be traced to the fact that the initial contraction of the jet, followed by the subsequent overexpansion downstream, might well, if enclosed in an exit cone, trap a region of dead air. The pressure in that would be different from the pressure at exit, and would therefore modify the contraction coefficient and, hence, the mass flow. He had referred to that possibility in the paper under Supercritical Flows, in connexion with the Borda mouth-piece; in that instance also the emergent jet might not always clear the outer lip downstream.

In regard to the shadowgraphs he was interested to note that they had recorded jet contraction at r equal to 0·23, even with an opening which was heavily countersunk upstream. They had also shown that the emergent angle of a nozzle jet, measured from the axis of the latter, had correlated well with the theoretical Prandtl–Meyer angle. For an orifice, sonic conditions at the lip (i.e. M equal to 1 in Fig. 1) were reached by fluid which was moving radially inwards. Hence, the theoretical curve of Fig. 8 would, in that instance, be shifted back 90 deg., indicating contraction, even at pressure ratios lower than 0·01. The corresponding shift for the modified orifice tested by them would be much less, as the countersink implied that the fluid would approach the lip obliquely. That angle would be even less than that of the countersink, owing to local separation at the shoulder, so that the upstream conditions were approaching those for a nozzle.

For the extreme case of an orifice discharging into a vacuum, Prandtl–Meyer theory suggested an inner contracting jet, surrounded by a very small mass of fluid which splayed outwards as in Fig. 46 of Howarth (1953). The motion of the latter would in practice be considerably modified by growth of boundary layer along the reservoir wall and he was unable to suggest any method of allowing for the expansion effect in that very limited region.

In the matter of recent information on contraction coefficients raised by Mr. Tantam, he hoped shortly to publish a further paper, which would enable velocity of approach effects to be accounted for.